



CENP-A overexpression promotes aneuploidy with karyotypic heterogeneity

Roshan Shrestha, Austin Rossi, Darawalee Wangsa, Ann Hogan, Kimberly Zaldana, Evelyn Suva, Yang Jo Chung, Chelsea Sanders, Simone Difilippantonio, Tatiana Karpova, et al.

► To cite this version:

Roshan Shrestha, Austin Rossi, Darawalee Wangsa, Ann Hogan, Kimberly Zaldana, et al.. CENP-A overexpression promotes aneuploidy with karyotypic heterogeneity. *Journal of Cell Biology*, 2021, 220 (4), pp.e202007195. 10.1083/jcb.202007195 . hal-03452721

HAL Id: hal-03452721

<https://cnrs.hal.science/hal-03452721>









Submitted on 29 Nov 2021

HAL is a multi-disciplinary open access archive for the deposit and dissemination of scientific research documents, whether they are published or not. The documents may come from teaching and research institutions in France or abroad, or from public or private research centers.

L'archive ouverte pluridisciplinaire **HAL**, est destinée au dépôt et à la diffusion de documents scientifiques de niveau recherche, publiés ou non, émanant des établissements d'enseignement et de recherche français ou étrangers, des laboratoires publics ou privés.

ARTICLE

CENP-A overexpression promotes aneuploidy with karyotypic heterogeneity

Roshan L. Shrestha¹ , Austin Rossi¹, Darawalee Wangsa¹, Ann K. Hogan³ , Kimberly S. Zaldana¹, Evelyn Suva¹, Yang Jo Chung¹, Chelsea L. Sanders², Simone Difilippantonio², Tatiana S. Karpova⁴ , Baktiar Karim² , Daniel R. Foltz³, Daniele Fachinetti⁵ , Peter D. Aplan¹ , Thomas Ried¹ , and Munira A. Basrai¹ 

Chromosomal instability (CIN) is a hallmark of many cancers. Restricting the localization of centromeric histone H3 variant CENP-A to centromeres prevents CIN. CENP-A overexpression (OE) and mislocalization have been observed in cancers and correlate with poor prognosis; however, the molecular consequences of CENP-A OE on CIN and aneuploidy have not been defined. Here, we show that CENP-A OE leads to its mislocalization and CIN with lagging chromosomes and micronuclei in pseudodiploid DLD1 cells and xenograft mouse model. CIN is due to reduced localization of proteins to the kinetochore, resulting in defects in kinetochore integrity and unstable kinetochore–microtubule attachments. CENP-A OE contributes to reduced expression of cell adhesion genes and higher invasion of DLD1 cells. We show that CENP-A OE contributes to aneuploidy with karyotypic heterogeneity in human cells and xenograft mouse model. In summary, our results provide a molecular link between CENP-A OE and aneuploidy, and suggest that karyotypic heterogeneity may contribute to the aggressive phenotype of CENP-A-overexpressing cancers.

Introduction

Chromosomal instability (CIN) refers to defects in chromosome segregation due to errors in mitosis. One of the main consequences of defective chromosome segregation is changes in the number of chromosomes (numerical CIN) and/or rearrangements in the genome (structural CIN), leading to genomic heterogeneity, a hallmark of cancer and drug resistance (Lee et al., 2011; Lim and Ma, 2019). Structural CIN can lead to segmental aneuploidy ranging from changes in few nucleotides to rearrangements of entire chromosomes, leading to deletions, translocations, inversions, and/or duplications as seen in malignancies, such as acute myeloid leukemia (Barnard et al., 1996; Geigl et al., 2008). Numerical CIN can lead to aneuploidy with loss or gain of whole chromosome, which has been observed in many solid cancers and hematological malignancies (Barnard et al., 1996; Maurici et al., 1998; Qi et al., 1996; Barnard et al., 2002; Paulsson and Johansson, 2007; Xu et al., 2016). Moreover, CIN is also associated with metastatic progression in several cancers (Turajlic and Swanton, 2016).

CIN, either numerical or structural, is mainly attributed to chromosome segregation defects during mitosis caused by

molecular alterations, such as multipolar spindles, defective sister chromatid cohesion, defects in chromosomes congression, replication stress, and improper/hyper-stable kinetochore–microtubule (KT-MT) attachments (Thompson et al., 2010; Gordon et al., 2012; Burrell et al., 2013). Kinetochores are assembled at the surface of the centromeres, which contain an evolutionarily conserved centromeric histone H3 variant—CENP-A in humans and Cse4 in budding yeast, Cid in flies—at α satellite DNA motifs interspersed with non-centromeric nucleosomes containing canonical histone H3 (Hasson et al., 2013; Henikoff et al., 2015). CENP-A is essential for centromere and kinetochore assembly (Perpelescu and Fukagawa, 2011; Guse et al., 2011). In addition, preexisting CENP-A marks the position and directs the recruitment of new CENP-A after DNA replication (Jansen et al., 2007). CENP-A is present at neocentromeres as well as in the majority of functional ectopic kinetochores (Mendiburo et al., 2011; Marshall et al., 2008; Nye et al., 2018), suggesting that it is an essential factor for centromere and kinetochore assembly (Perpelescu and Fukagawa, 2011; Guse et al., 2011). CENP-A is the foundation for the

¹Genetics Branch, Center for Cancer Research, National Cancer Institute, National Institutes of Health, Bethesda, MD; ²Laboratory Animal Sciences Program, Frederick National Laboratory for Cancer Research, Leidos Biomedical Research, Frederick, MD; ³Department of Biochemistry and Molecular Genetics, Northwestern University, Chicago, IL; ⁴Laboratory of Receptor Biology and Gene Expression, Center for Cancer Research, National Cancer Institute, National Institutes of Health, Bethesda, MD; ⁵Institut Curie, PSL Research University, Centre National de la Recherche Scientifique, Unité Mixte de Recherche 144, Paris, France.

Correspondence to Munira A. Basrai: basraim@nih.gov.

© 2021 Shrestha et al. This article is distributed under the terms of an Attribution–Noncommercial–Share Alike–No Mirror Sites license for the first six months after the publication date (see <http://www.rupress.org/terms/>). After six months it is available under a Creative Commons License (Attribution–Noncommercial–Share Alike 4.0 International license, as described at <https://creativecommons.org/licenses/by-nc-sa/4.0/>).

recruitment of most of the constitutive centromere-associated network (CCAN; Okada et al., 2006; Foltz et al., 2006). CCAN constitutes 16 centromeric proteins that link CENP-A with outer kinetochore proteins that mediate attachment to microtubules. CENP-A stably associates with CENP-C (Carroll et al., 2010), a component of the CCAN that connects with Mis12 (Screpanti et al., 2011), a component of the outer kinetochore complex, KNL1/Mis12/Ndc80. CENP-T, a component of the CENP-S/T/W/X complex has a histone-like domain that associates with centromeric DNA and links the inner and outer kinetochores by associating with Spc24/25 of the Ndc80 complex and Mis12 (Hori et al., 2008; Nishino et al., 2013; Nishino et al., 2012; Huis In 't Veld et al., 2016). Moreover, CENP-C and CENP-T are also responsible for recruiting the Ndc80 complex to kinetochores (Suzuki et al., 2015). Once the microtubules establish stable end-on attachment with kinetochores, the microtubule plus end-associated protein, Astrin, gets recruited to kinetochores through Aurora B activity (Schmidt et al., 2010; Shrestha and Draviam, 2013; Shrestha et al., 2017b). The cooperative functions of the CCAN network and kinetochore-associated proteins facilitate proper KT-MT attachment and faithful chromosome segregation.

The centromeric localization of CENP-A is cell-cycle regulated. During DNA replication in S-phase, the CENP-A pool gets diluted to be distributed into two sister chromatids (Jansen et al., 2007); however, at this stage the CENP-A chaperone, holiday junction recognition protein (HJURP), interacts with MCM2 and associates with centromeres to retain the centromeric pool of CENP-A (Dunleavy et al., 2009; Foltz et al., 2009; Pan et al., 2019; Zasadzinska et al., 2018; Müller et al., 2014; Nechemia-Arbely et al., 2019). Additionally, DNA replication-independent recruitment of new CENP-A at G1 phase of the cell cycle is also mediated by HJURP and its interaction with Mis18 β (Nardi et al., 2016; Barnhart-Dailey et al., 2017). Alternatively, CENP-C-mediated recruitment of Mis18BP1 at metaphase centromeres promotes the deposition of new CENP-A at centromeres in the G1 phase of the cell cycle (Moree et al., 2011). DNA replication also acts as a mechanism for maintaining centromere identity by removing CENP-A that is mislocalized at the non-centromeric regions (Nechemia-Arbely et al., 2019).

Defining consequences of CENP-A mislocalization is an area of active investigation. Studies with budding yeast and flies have shown that mislocalization of CENP-A to non-centromeric regions leads to chromosome segregation defects (Au et al., 2008; Choi et al., 2012; Heun et al., 2006), and that defects in ubiquitin proteasome-mediated proteolysis of CENP-A contribute to its mislocalization in budding yeast (Ranjitkar et al., 2010; Hewawasam et al., 2010; Au et al., 2013; Deyter and Biggins, 2014; Ohkuni et al., 2014; Ohkuni et al., 2016; Cheng et al., 2016; Ciftci-Yilmaz et al., 2018; Au et al., 2020; Eisenstatt et al., 2020; Ohkuni et al., 2020). Studies from our laboratory and those of others have shown that mislocalization of overexpressed CENP-A to non-centromeric regions contributes to CIN in HeLa and colorectal cancer cells (Athwal et al., 2015; Van Hooser et al., 2001; Nye et al., 2018; Shrestha et al., 2017a). Increased expression of CENP-A has been observed in many cancers, including hepatocellular carcinomas, glioblastomas, and

different breast cancer subtypes (Sun et al., 2016; Li et al., 2011; Stangeland et al., 2015; McGovern et al., 2012; Zhang et al., 2016; Rajput et al., 2011; Tomonaga et al., 2003). CENP-A overexpression (OE) has been linked to decreased overall survival, higher tumor grades, increased invasiveness, higher risk of disease progression, and poor patient response to therapy (Zhang et al., 2016; Saha et al., 2020). Bioinformatic analyses have reported increased expression of CENP-A and kinetochore components in breast cancer samples with aneuploidy (Pfister et al., 2018); however, the molecular consequences of CENP-A OE on CIN and aneuploidy have not been defined. Given the correlation of increased expression of CENP-A with cancer, it is important to understand how CENP-A OE and subsequent mislocalization contributes to aneuploidy.

In this study, we used a colorectal pseudodiploid cancer cell line, DLD1, and a xenograft mouse model to investigate the molecular consequences of CENP-A OE on CIN and aneuploidy. Our results showed that CENP-A OE leads to mislocalization of CENP-A to non-centromeric regions, CIN phenotypes (lagging chromosomes, micronuclei), and aneuploidy with karyotypic heterogeneity in DLD1 cells and xenograft mouse model. We determined that CIN phenotypes in CENP-A-overexpressing cells were due to reduced localization of a subset of centromeric and kinetochore proteins, which contribute to defects in kinetochore integrity and unstable KT-MT attachments. Our studies provide the first evidence for a molecular link between CENP-A OE and mislocalization to aneuploidy with karyotypic heterogeneity. We propose that karyotypic heterogeneity may contribute to the aggressive phenotype with poor prognosis and therapy resistance in CENP-A-overexpressing cancers.

Results

CENP-A OE contributes to mislocalization of CENP-A and CENP-C to non-centromeric regions and chromosome mis-segregation in DLD1 cells

To investigate the molecular consequences of CENP-A OE on CIN and aneuploidy, we examined the levels of endogenous CENP-A in different cell lines. Western blot analysis showed the comparable levels of CENP-A expression in HeLa, RPE, HEK293T, and MDA-MB-231, but expression of CENP-A was reduced in the pseudodiploid colorectal cancer cell line, DLD1 (Fig. S1 A). Reduced levels of CENP-A in DLD1 cells compared with that in other colorectal cancer cells has been previously reported (Athwal et al., 2015). The reduced expression of CENP-A and the pseudodiploid nature of DLD1 cells made it an ideal cell line to investigate the consequences due to inducible OE of CENP-A. We pursued further studies with DLD1 with inducible expression of YFP-tagged CENP-A from a doxycycline (DOX)-inducible promoter (DLD1^{CENP-A}). We optimized the conditions for OE of YFP-CENP-A in DLD1^{CENP-A} cells and determined that treatment of cells with 0.1 μ g/ml DOX concentration for 30 min, followed by removal of DOX and further growth of cells for 20 h showed the highest levels of exogenous CENP-A (Fig. S1 B). Next, we compared the levels of exogenously OE CENP-A, 20 h post-DOX removal, in DLD1^{CENP-A} cells with the levels of endogenous CENP-A in cell lines, as in Fig. S1 A. We determined that the

levels of OE CENP-A in DLD1^{CENP-A} cells with DOX were ~25-fold higher than the levels of endogenous CENP-A in non-transformed cell line RPE1 (Fig. S1 C). Based on these results, all experiments, unless otherwise stated, were performed with cells treated with 0.1 µg/ml DOX for 30 min and within 20–25 h post-DOX wash (Fig. S1 D). To examine for possible cell-to-cell variation in the expression of CENP-A, we measured the signal intensity of CENP-A in at least 250 interphase DLD1^{CENP-A} cells with or without DOX treatment. As expected, CENP-A signal intensity was low and uniform across DLD1^{CENP-A} cells without DOX treatment (Fig. S1 E). The CENP-A signal intensity in a majority of DLD1^{CENP-A} cells with DOX treatment was uniformly higher, with the exception of some cells with very high CENP-A signal intensity. There was significant difference in CENP-A signal intensity ($P < 0.0001$, Fig. S1 E) between DOX-treated DLD1^{CENP-A} cells compared with control cells. We next examined whether OE of CENP-A contributes to defects in cell-cycle progression or cell proliferation in the experimental set up, as in Fig. S1 D. Flow cytometry analysis of cells stained with DAPI for DNA and 5-ethyl-2'-deoxyuridine (EdU) for newly synthesized DNA showed similar distribution of cells in S, G1, and G2M phase in DLD1^{CENP-A} cells with or without DOX treatment (Fig. S2, A and B), thereby confirming normal proliferation and cell-cycle progression of cells upon CENP-A OE.

We next examined the localization of CENP-A in DLD1^{CENP-A} cells treated with 0.1 µg/ml DOX according to the regimen in Fig. S1 D by using chromosome spreads from metaphase cells. Cells were immunostained with anti-CENP-A antibody for centromeres and stained with DAPI for chromosomes. We defined the centromeric region as the constriction site of a chromosome with the brightest signal of CENP-A, whereas the non-centromeric region is any other region on the chromosome arms beyond the constriction site. Our results showed that, as expected, CENP-A localized to centromeres in both DLD1^{CENP-A} cells with and without DOX treatment; however, CENP-A also localized to non-centromeric regions in DLD1^{CENP-A} cells with DOX treatment, but was barely detectable at these sites in control DLD1^{CENP-A} cells without DOX treatment (Fig. 1 A). Quantitative analysis showed significantly high levels of non-centromeric CENP-A signals in DOX-treated DLD1^{CENP-A} cells (Fig. 1 B). Based on these results, we conclude that overexpressed CENP-A mislocalizes to non-centromeric regions in DLD1^{CENP-A} cells. We previously reported that CENP-C, a component of the CCAN network that interacts with CENP-A, mislocalizes to noncentromeric regions in HeLa cells with CENP-A OE (Shrestha et al., 2017a; Van Hooser et al., 2001). Hence, we examined the effect of CENP-A OE on the localization of endogenous CENP-C by using chromosome spreads. CENP-C was mislocalized to non-centromeric regions in DLD1^{CENP-A} cells with DOX treatment (Fig. 1 C). Quantitative analysis showed significantly higher signal intensity of CENP-C at non-centromeric regions in DLD1^{CENP-A} cells with DOX treatment compared with control DLD1^{CENP-A} cells without DOX treatment (Fig. 1 D). Intriguingly, we also observed significantly reduced levels of CENP-C at centromeric regions in DOX-treated DLD1^{CENP-A} cells compared with that in control DLD1^{CENP-A} cells (Fig. 1 D).

We next examined the consequences due to mislocalization of CENP-A and CENP-C on chromosome segregation in DOX-

treated DLD1^{CENP-A} cells. Analysis of time-lapse movies (Video 1) and immunostained images showed that a significant proportion of DOX-treated DLD1^{CENP-A} cells exited mitosis with defective chromosome segregation (lagging chromosomes, uncongressed chromosomes, and DNA bridges; Fig. 1, E and F). To rule out an effect of DOX treatment on chromosome segregation, we examined the status of chromosome segregation in parental DLD1 cells with or without DOX. YFP-CENP-A expression and mislocalization were not detected in DOX-treated parental DLD1 cells, and these cells did not exhibit chromosome segregation defects (Fig. S2, C and D). Hence, DOX treatment alone does not contribute to CENP-A mislocalization and CIN phenotypes in DLD1 cells. Based on these results, we conclude that CENP-A OE contributes to mislocalization of CENP-A and CENP-C and CIN phenotypes.

Increased incidence of micronuclei with ruptured nuclear membrane in DLD1 cells with CENP-A OE

Chromosome segregation defects have been shown to contribute to the formation of micronuclei (Cimini et al., 2002); therefore, the defects in chromosome segregation due to CENP-A OE led us to examine the incidence of micronuclei in DOX-treated DLD1^{CENP-A} cells. Time-lapse movies (Video 2) and immunostained images showed that the proportion of cells with micronuclei was significantly higher in DOX-treated DLD1^{CENP-A} cells compared with control DLD1^{CENP-A} cells without DOX treatment (Fig. 2, A and B). Defects in nuclear lamina assembly that cause loss of compartmentalization during interphase is a common fate for micronuclei (Hatch et al., 2013). We used Lamin B, a nuclear lamin protein that localizes to the inner nuclear membrane as a marker to examine the status of the nuclear membrane of micronuclei in DLD1^{CENP-A} cells with or without DOX treatment. We scored micronuclei with normal nuclear membrane (Lamin B intact), ruptured nuclear membrane (Lamin B partial), or without nuclear membrane (Lamin B absent; Fig. 2 C). Our results showed that the incidence of micronuclei with ruptured nuclear membrane was significantly higher in DOX-treated DLD1^{CENP-A} cells compared with control DLD1^{CENP-A} cells without DOX treatment (Fig. 2 D). Micronuclei with no nuclear membrane were similar in both DOX-treated and control DLD1^{CENP-A} cells (Fig. 2 D). These results show that CENP-A OE contributes to CIN and increased incidences of micronuclei with ruptured nuclear membrane.

Reduced localization of proteins at kinetochore in cells with CENP-A OE

We hypothesized that since CENP-A is the basis for the assembly of the kinetochore, its mislocalization may affect the localization of other centromeric and kinetochore-associated proteins, and this may be the underlying molecular basis for the CIN phenotypes in CENP-A-overexpressing cells. Support for this hypothesis is based on the reduced localization of a CCAN component, CENP-C, at centromeres in cells with CENP-A OE. To further explore the hypothesis, we examined the localization of a subset of centromeric and kinetochore-associated proteins, such as CENP-T, NUF2, and Mis12, that are required for faithful chromosome segregation. We examined the localization of

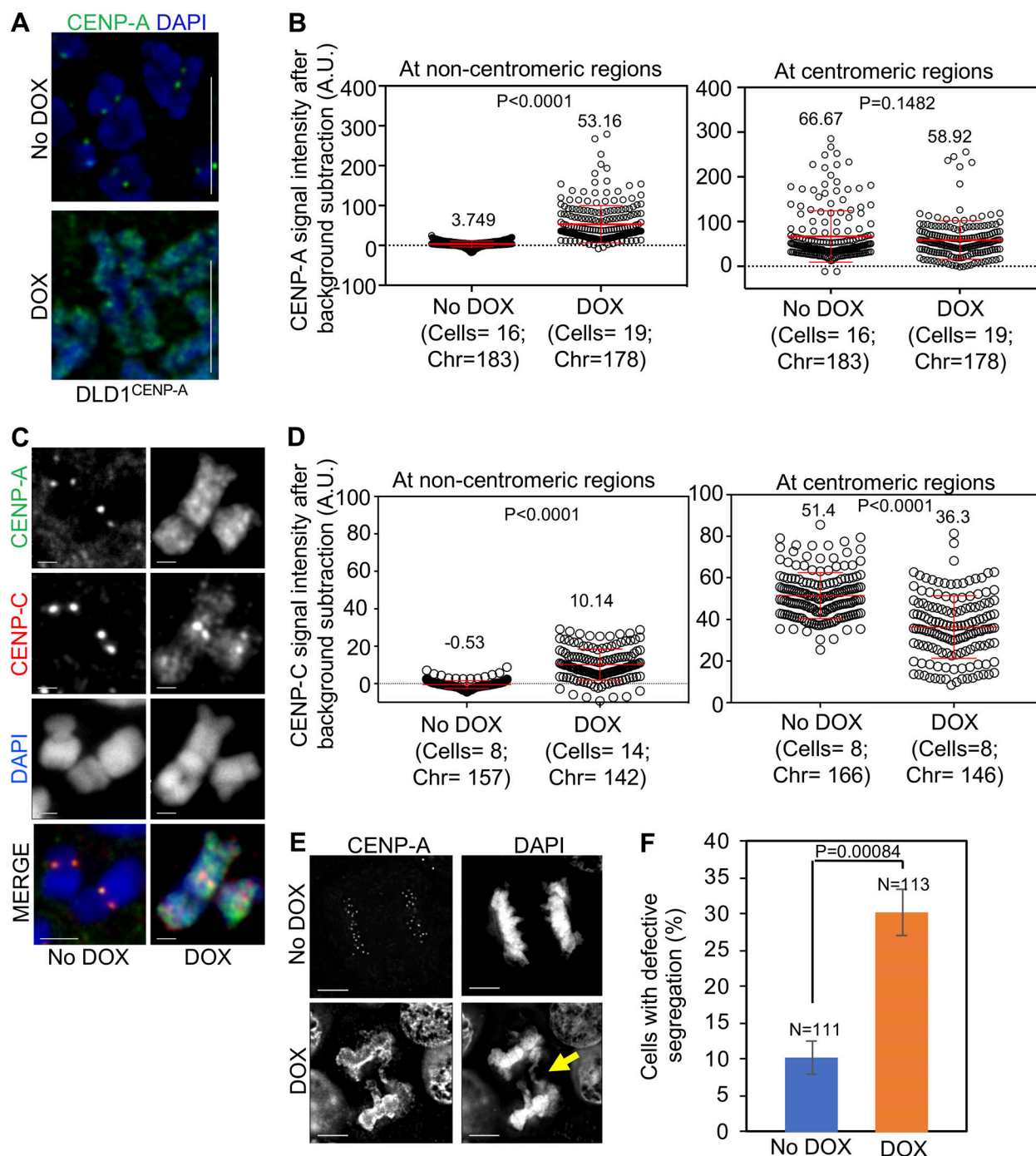


Figure 1. Overexpression of CENP-A contributes to mislocalization of CENP-A and CENP-C to non-centromeric regions and chromosome mis-segregation in DLD1 cells. (A) Inducible OE of YFP-CENP-A leads to its mislocalization to chromosome arms in DLD1 cells. Chromosome spread images showing localization of CENP-A to centromeres in DLD1^{CENP-A} cells without DOX treatment and to chromosome arms in cells with DOX treatment. Following preparation of chromosome spreads, cells were fixed in 4% PFA, followed by trypsinization with 0.1% Triton X-100 in PBS. Cells were immunostained with antibody against CENP-A and stained with DAPI. Scale bar: 2 μ m. (B) Prism graphs for quantification of CENP-A signal intensities at non-centromeric (left) and centromeric (right) regions in chromosome spreads of DLD1^{CENP-A} cells from A. Each circle represents a spot on a chromosome. "Cells" and "chr" denote number of cells and chromosomes analyzed, respectively. Red horizontal lines represent mean signal intensity as indicated. Error bars represent SD across areas measured in number of cells from three independent experiments. P values were calculated by using the Mann-Whitney U test. (C) Reduced levels of CENP-C at centromeres with mislocalization to chromosome arms in DLD1 cells overexpressing CENP-A. Chromosome spread images show localization of CENP-C in DLD1^{CENP-A} cells with or without DOX treatment, followed by immunostaining with antibodies against CENP-A and CENP-C, staining with DAPI, and analysis for CENP-C signal intensity at centromeric and non-centromeric regions. Scale bar: 2 μ m. (D) Prism graphs for quantification of CENP-C signal intensities at non-centromeric (left) and centromeric (right) regions in chromosome spreads of DLD1^{CENP-A} cells treated as in C. Each circle represents a spot on a chromosome. "Cells" and "chr" denote number of cells and chromosomes analyzed, respectively. Red horizontal lines represent mean signal intensity as indicated. Error bars represent SD across areas measured in number of cells from two independent experiments. P values were calculated by using the

Mann-Whitney *U* test. **(E)** Increased chromosome segregation defects in DLD1 cells with overexpressed and mislocalized CENP-A. Images show chromosome segregation status in DLD1^{CENP-A} cells with or without DOX treatment. Cells were immunostained with antibodies against CENP-A, stained with DAPI, and analyzed for chromosome segregation status. Yellow arrow shows missegregated chromosomes in DOX-treated DLD1^{CENP-A} cells. Scale bar: 5 μ m. **(F)** Quantification shows the proportion of cells with defective chromosome segregation in DLD1^{CENP-A} cells treated as in E. Error bars represent SEM from three independent experiments. *P* values were calculated by using the unpaired Student's *t* test.

CENP-T, another component of the CCAN network that directly associates with centromeric DNA and is required for proper chromosome segregation (Hori et al., 2008; Nishino et al., 2012). Quantitative analysis for localization of CENP-T on the metaphase plate of bipolar cells showed significantly reduced CENP-T signal intensity at centromeres in DLD1^{CENP-A} cells with DOX compared with that in control DLD1^{CENP-A} cells without DOX (Fig. 3, A and B; and Fig. S3 A). These results show that CENP-A OE contributes to reduced levels of two major components of the CCAN network, CENP-C and CENP-T at centromeres.

Depletions of CENP-C and CENP-T affect the proper recruitment of outer kinetochore proteins Mis12 and Ndc80 complexes to kinetochores (Gascoigne et al., 2011; Screpanti et al., 2011; Hori et al., 2008; Przewłoka et al., 2011; Suzuki et al., 2015). Hence, we examined the localization of NUF2, a component of the Ndc80 complex, and Mis12, a component of Mis12 complex, in cells with CENP-A OE. Quantitative analysis for the signal intensities of NUF2 (Fig. 3, C and D; and Fig. S3 B) and Mis12 (Fig. 3, E and F; and Fig. S3 C) showed reduced levels of these proteins at kinetochores in DLD1^{CENP-A} cells with DOX compared with that in control DLD1^{CENP-A} cells without DOX. Furthermore, we did not observe mislocalization of CENP-T, NUF2, HEC1, or Mis12 at non-centromeric regions in these cells. It is possible that these proteins do not get mislocalized or the levels of mislocalization are below the sensitivity of the assay. Taken together, with these results we conclude that CENP-A OE and mislocalization contribute to the mislocalization of CENP-C, CENP-T, NUF2, and Mis12 at centromeres and kinetochores.

CENP-A OE weakens the strength of kinetochores and contributes to reduced stable end-on attachment between kinetochores and microtubules

The outer kinetochore is the platform for the interaction of kinetochores with microtubules, and once microtubules are stably attached, they pull the sister chromatids apart during anaphase (Mitchison and Salmon, 1992; Gorbsky and Borisy, 1989; Cheeseman et al., 2006). The reduced localization of components of outer kinetochore proteins, such as NUF2 and Mis12, which regulate KT-MT attachments, in CENP-A-overexpressing cells led us to propose that CENP-A OE may affect the integrity of kinetochores. Defects in kinetochore integrity results in a reduced interkinetochore distance between sister chromatids (Uchida et al., 2009). Reduced interkinetochore distance is a proxy for reduced pulling force between two sister chromatids due to unstable KT-MT interactions (Shrestha et al., 2017a). Hence, we measured the interkinetochore distance in DLD1^{CENP-A} cells with or without DOX treatment. NUF2 signal was used as an outer kinetochore marker, and the distance between two NUF2 signals on a pair of kinetochores was measured as the

interkinetochore distance. We determined that the interkinetochore distance was reduced in DOX-treated DLD1^{CENP-A} cells compared with control DLD1^{CENP-A} cells (Fig. 4, A and B). These results show that CENP-A OE and mislocalization weaken the endogenous kinetochores, leading to defects in kinetochore integrity in DOX-treated DLD1^{CENP-A} cells.

Reduced interkinetochore distance and low levels of NUF2 and Mis12 at kinetochores in CENP-A-overexpressing cells prompted us to examine if the physical attachments between kinetochores and microtubules are affected in these cells. Previous studies have shown that those microtubules that are not stably attached to kinetochores destabilize upon exposure to cold temperature, resulting in kinetochores without microtubule occupancy (Brady et al., 1984). We exploited this characteristic feature of microtubules and used the cold-resistant stable microtubule assay to examine the status of KT-MT attachments in cells with CENP-A OE. For clear visualization of kinetochores and associated microtubule bundles, we treated cells with monastrol and MG132 to obtain mitotically arrested monopolar cells, followed by exposure to ice for 10 min (Shrestha and Draviam, 2013). Following immunostaining, cells were analyzed for the kinetochores that were end-on attached to microtubules or non-end-on attached (kinetochores without microtubules or kinetochores that are laterally attached to microtubules; Fig. 4 C). Our results showed that a significantly higher proportion of kinetochores in DOX-treated DLD1^{CENP-A} cells were non-end-on attached to microtubules compared with control DLD1^{CENP-A} cells (Fig. 4, C and D; and Fig. S4 A). Hence, we propose that reduced stable end-on attachments between KT-MT contribute to improper pulling of chromatids and reduced interkinetochore distance in cells overexpressing CENP-A.

Previous studies have shown that the Astrin/SKAP complex is recruited to kinetochores once microtubules establish stable end-on attachment with the kinetochores (Shrestha et al., 2017b); therefore, we used the status of Astrin at kinetochores as a marker to distinguish end-on KT-MT attachments from non-end-on KT-MT attachments. Cold-exposed, mitotically arrested monopolar cells (monastrol treated), as in Fig. 4 C, were immunostained for HEC1, an outer kinetochore protein and Astrin. We quantified kinetochores (marked by HEC1) that are positive for Astrin (stable end-on KT-MT attachment) or devoid of Astrin (lacking or unstable KT-MT attachments; Fig. 4 E). This analysis showed that the proportion of kinetochores that were positive for Astrin signal at kinetochores was significantly reduced in DOX-treated DLD1^{CENP-A} cells compared with control DLD1^{CENP-A} cells (Fig. 4, E and F; Video 3; and Video 4). Additionally, the signal intensity of HEC1 at kinetochores was reduced in DOX-treated DLD1^{CENP-A} cells (Fig. 4 E and Fig. S4 B). These observations are consistent with the reduced signal

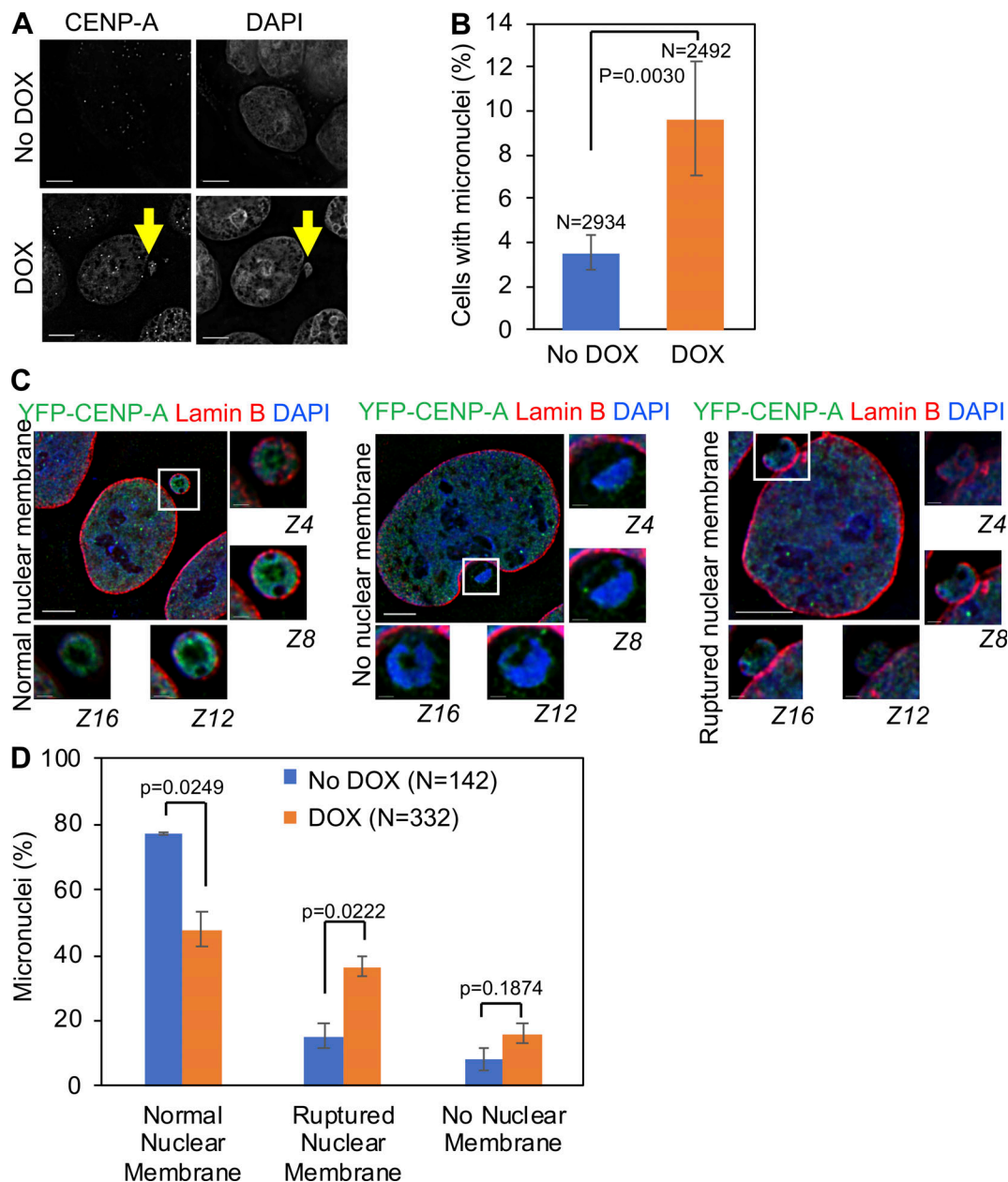


Figure 2. Overexpressed CENP-A contributes to increased incidence of micronuclei with ruptured nuclear membrane in DLD1 cells. (A) Increased incidence of micronuclei in DLD1 cells with overexpressed and mislocalized CENP-A. Images show micronuclei in DLD1^{CENP-A} cells with or without DOX treatment. Cells were immunostained with antibodies against CENP-A, stained with DAPI, and analyzed for the presence of micronuclei. Yellow arrows show micronuclei in DOX-treated DLD1^{CENP-A} cells. Scale bar: 5 μ m. (B) Quantification of images from A shows the incidence of micronuclei in DLD1^{CENP-A} cells with or without DOX treatment. (C) Micronuclei with different status of nuclear membrane in DLD1 cells with overexpressed and mislocalized CENP-A. Images show micronuclei with normal nuclear membrane, ruptured nuclear membrane, or no nuclear membrane in DLD1^{CENP-A} cells with DOX treatment. Cells were immunostained with antibodies against CENP-A and Lamin B and stained with DAPI. Insets correspond to the z-stacks from the white-boxed area in the main figure. Scale bar: 5 μ m (main image), 1 μ m (insets). (D) Quantification shows the proportion of micronuclei with different status of nuclear membrane in DLD1^{CENP-A} cells with or without DOX treatment. Error bars in B and D represent SEM from three independent experiments. P values were calculated using the unpaired Student's t test.

intensity of NUF2 due to CENP-A OE (Fig. 3, C and D), because both HEC1 and NUF2 are components of the outer kinetochore Ndc80 complex. To further confirm the unstable KT-MT attachments in DOX-treated DLD1^{CENP-A} cells, we examined the signal intensity of Astrin at congressed kinetochores at the metaphase plate in bipolar cells without exposure to cold and

monastrol. Our results showed that Astrin signal intensity at congressed kinetochores was significantly reduced in DOX-treated DLD1^{CENP-A} cells compared with control DLD1^{CENP-A} cells (Fig. S4, C and D). We conclude that CENP-A OE weakens the strength of kinetochores and contributes to reduced stable end-on attachment between kinetochores and microtubules.

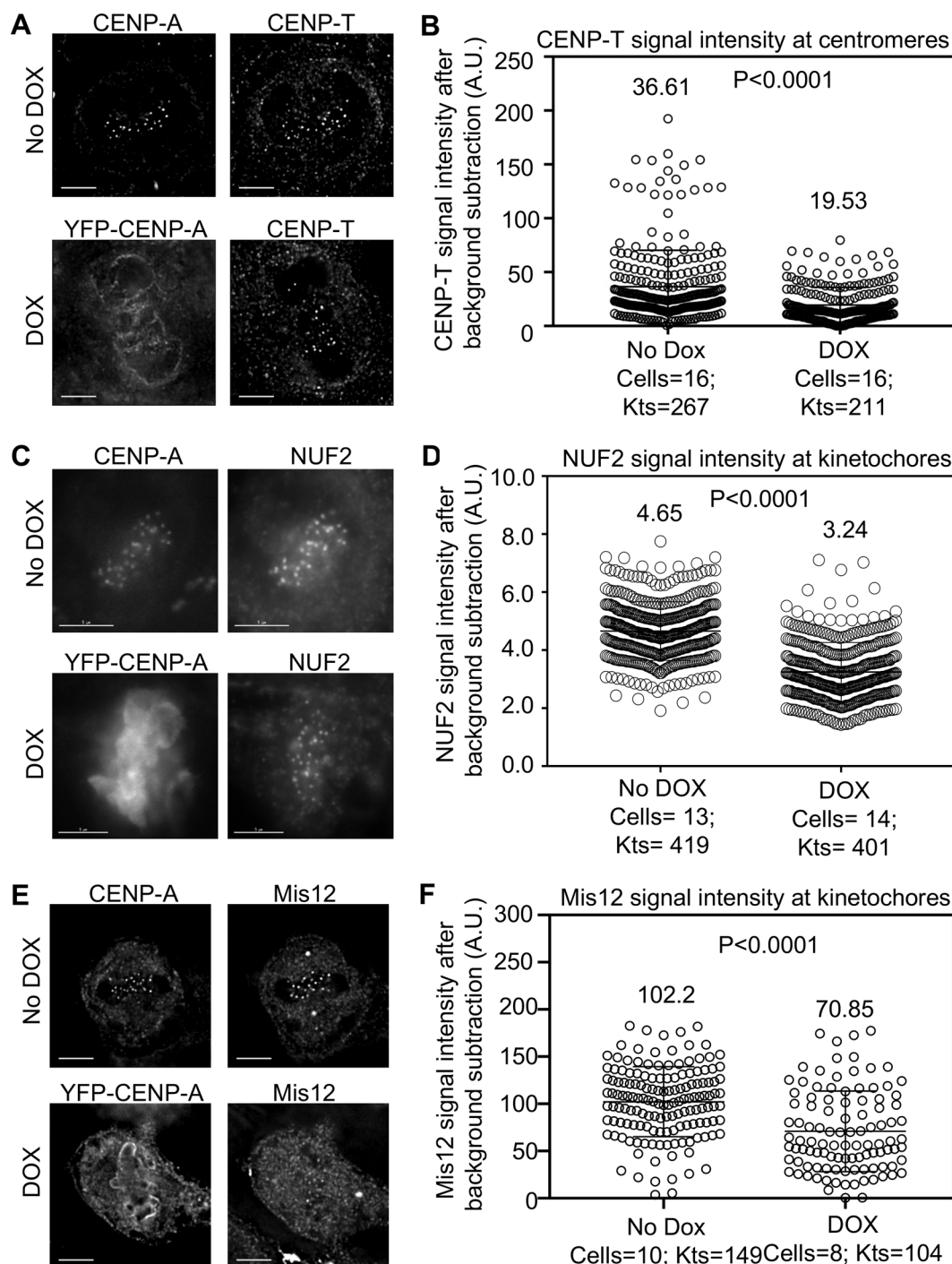


Figure 3. Reduced localization of proteins at kinetochore in cells with CENP-A OE. (A and B) Reduced CENP-T signal intensities in DLD1 cells with overexpressed and mislocalized CENP-A. Images (A) of CENP-T localization at centromeres on metaphase plates, and prism graph (B) shows CENP-T signal intensity at centromeres in DLD1^{CENP-A} cells with or without DOX treatment. **(C and D)** Reduced NUF2 signal intensities in DLD1 cells with overexpressed and mislocalized CENP-A. Images (C) of NUF2 localization at kinetochores on metaphase plates, and prism graph (D) shows NUF2 signal intensity at kinetochores in DLD1^{CENP-A} cells with or without DOX treatment. **(E and F)** Reduced levels of Mis12 at centromeres in DLD1 cells with overexpressed CENP-A. Images (E) of localization of Mis12 at kinetochores on metaphase plates, and prism graph (D) shows Mis12 signal intensity at kinetochores in DLD1^{CENP-A} cells with or without DOX treatment. For all experiments in this figure, before immunostaining, cells were treated with 10 μ M MG132 for 90 min, followed by fixation with ice-cold methanol for 1 min, and then immunostaining with antibodies as indicated. Cells were stained with DAPI and analyzed for signal intensities at kinetochores on metaphase plates. For all prism graphs in B, D, and F, each circle represents each kinetochore pair and “Kts” denotes the number of kinetochore pairs analyzed in a certain number of cells as denoted by “Cells.” Red horizontal lines represent mean signal intensities as indicated. Error bars represent SD measured across kinetochores in the indicated number of cells from three independent experiments. P values were calculated by using the Mann-Whitney *U* test. Scale bar: 5 μ m.

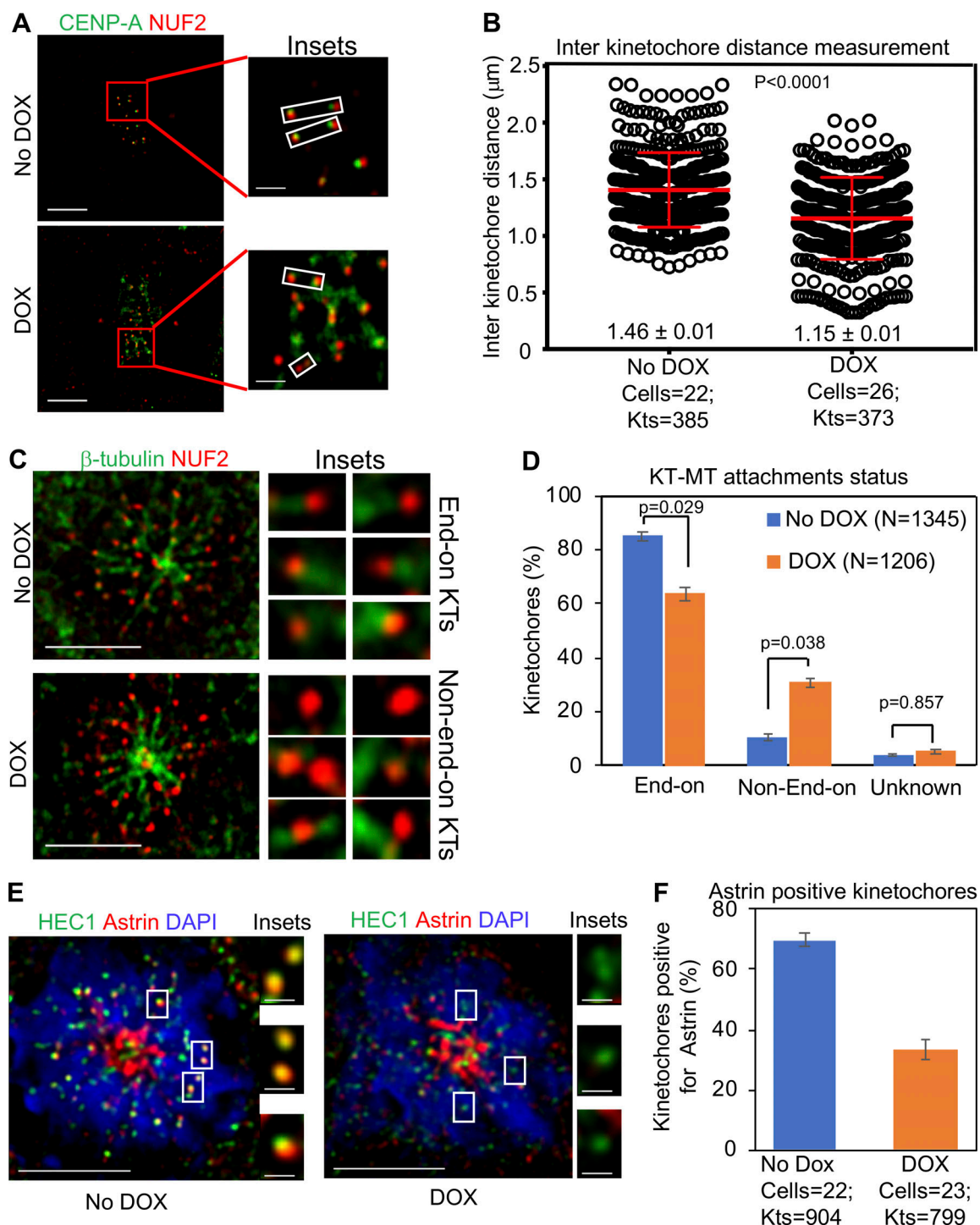


Figure 4. CENP-A OE weakens the strength of kinetochores and contributes to reduced stable end-on attachment between kinetochores and microtubules. (A) Reduced interkinetochore distance in DLD1 cells due to weakening of native kinetochores in DLD1 cells overexpressing CENP-A. Images show interkinetochore distance in DLD1^{CENP-A} cells with or without DOX treatment. Prior to immunostaining, cells were treated with 10 μM MG132 for 90 min. Cells were immunostained with antibodies against CENP-A and NUF2, stained with DAPI, and analyzed for interkinetochore distance as determined by the distance between two NUF2 signals in a pair of chromatids. Insets correspond to red-boxed areas in main images. White-boxed areas in insets show examples for kinetochore pairs included in the analysis. Scale bar: 5 μm . (B) Prism graph for quantification of interkinetochore distance in DLD1^{CENP-A} cells with or without DOX treatment. Red horizontal lines represent mean interkinetochore distance. Error bars represent SD across kinetochores measured in the indicated number of cells from three independent experiments. P values were calculated by using the Mann-Whitney U test. (C) Reduced levels of stable end-on attached kinetochores in DLD1 cells overexpressing CENP-A. Images show KT-MT attachments status in DLD1^{CENP-A} cells with or without DOX treatment. Prior to fixation with ice-cold methanol for 1 min, cells were treated with 10 μM monastrol (3 h) and 10 μM MG132 (90 min), followed by exposure to cold for 10 min. Cells were immunostained with antibodies against NUF2 and β -tubulin and analyzed for kinetochores with end-on (stable and cold resistant) or non-end-on attachment (unstable and cold sensitive) to microtubules. Insets show end-on and non-end-on KT-MT attachment status. Scale bar: 5 μm (main figures).

(D) Quantification shows KT-MT attachments status in DLD1^{CENP-A} cells with or without DOX treatment from C. (E) Reduced levels of Astrin-positive kinetochores in DLD1 cells with overexpressed CENP-A. Images show status of Astrin at kinetochores in DLD1^{CENP-A} cells with or without DOX treatment, following the experimental regimen as in C. Cells were immunostained with antibodies against HEC1 and Astrin, stained with DAPI, and analyzed for kinetochores with or without Astrin, which represents end-on versus non-end-on KT-MT attachments, respectively. Insets correspond to white-boxed areas in main images. Scale bar: 5 μ m (main images), 0.5 μ m (insets). (F) Quantification shows Astrin-positive kinetochores in DLD1^{CENP-A} cells with or without DOX treatment. "Kts" denotes the number of kinetochore pairs analyzed in the indicated number of cells as denoted by "Cells." Error bars in D and F represent SEM from three independent experiments. P values calculated by using the proportion test (D) and unpaired Student's *t* test (F) are indicated.

Reduced expression of cell adhesion genes and higher invasion of cells with CENP-A OE

Since CENP-A OE leads to mislocalization of CENP-A to non-centromeric regions and CIN, we examined whether transcriptional changes due to CENP-A OE contribute to the CIN phenotype. RNA sequencing (RNaseq) was used to compare the transcriptomes of DLD1^{CENP-A} cells with or without DOX treatment. Overall, the majority of gene expression changes resulting from CENP-A OE were less than twofold (Fig. 5 A). Expression of *E2F1*, *FOXM1*, and *MYBL2*, genes that were previously found to drive aneuploidy, was not significantly altered in cells with CENP-A OE (Fig. 5 A, yellow box; Pfister et al., 2018; Zhang et al., 2016). The small changes in gene expression are consistent with previous studies showing a limited effect on gene expression in HeLa cells with constitutive OE of CENP-A (Lacoste et al., 2014).

We next performed gene set enrichment analysis (GSEA) by using the Reactome and KEGG canonical pathways gene set collections (Broad Institute; Subramanian et al., 2005). GSEA analysis showed an enrichment of five gene sets—mitotic prometaphase, mitotic G1 G1 S phases, mitotic M M G1 phases, mitotic G2 G2 M phases, and cell-cycle mitotic—related to mitosis among genes that are upregulated in cells with CENP-A OE (Fig. 5, B and C). GSEA analysis of published RNaseq data from HeLa cells with constitutive OE of CENP-A also demonstrated an enrichment of mitosis-related gene sets among upregulated genes following CENP-A OE (Fig. 5, B and C; Lacoste et al., 2014). We note that upregulation of mitotic genes is a signature of aneuploidy and CIN in tumors and may drive aneuploidy (Pfister et al., 2018; How et al., 2015; Carter et al., 2006).

Our results showed that one of the consequences of CENP-A OE was reduced levels of a subset of centromeric and kinetochore proteins at the centromeres (Figs. 1 and 3). We reasoned that this may be due to local defects at the centromere and kinetochore, or due to reduced expression of the corresponding genes. Hence, we analyzed the RNaseq data for the expression of CENP-C, CENP-T, NUF2, and Mis12, which were reduced at centromere and kinetochores in CENP-A OE cells. Our results showed that the expression of genes encoding these proteins is not significantly affected upon CENP-A OE in DLD1^{CENP-A} cells (Fig. 5 D). Hence, we conclude that CENP-A OE contributes to defects in kinetochore integrity and reduced levels of CENP-C, CENP-T, Nuf2, and Mis12 proteins at the centromeres and kinetochores, leading to CIN phenotype.

GSEA analysis also showed that three gene sets related to cell adhesion (adherens junction interactions, cell adhesion molecules [CAMs], cell-cell junction organization) were significantly enriched among the genes downregulated in cells with CENP-A OE (Fig. 5 B). Consistent with our results, downregulation of genes in all three cell adhesion gene sets was observed in HeLa

cells with CENP-A OE (Fig. 5, B and C). Our results and those of Lacoste et al. (2014) demonstrate that CENP-A OE contributes to downregulation of genes related to cell adhesion in HeLa and DLD1 cells. Several studies have reported that reduced expression of CAMs correlates with increased invasiveness (Kinsella et al., 1994; Mierke et al., 2010; Moh and Shen, 2009). The results for RNaseq analysis showed reduced expression of CAMs in cells with CENP-A OE. Furthermore, CENP-A-overexpressing cancers are highly invasive (Ma et al., 2003; Rajput et al., 2011) with poor prognosis (Wang et al., 2005). Hence, we examined the effects of CENP-A OE on cell invasion in DLD1 cells by using a trans-well invasion assay. Cells were seeded in a trans-well with matrigel and invasiveness was quantified by counting cells that migrate to the bottom of the trans-well after 16 h (Fig. 6 A). We observed 2.5-fold higher invasion of DOX-treated DLD1^{CENP-A} cells into the matrigel compared with control cells (Fig. 6, B and C). A 2.5-fold increase in invasiveness in DLD1 cells was significant, as reported in previous studies (Zhou et al., 2018). These results show that CENP-A OE contributes to increased invasiveness of DLD1 cells.

Depletion of the histone chaperone DAXX partially suppresses the mislocalization of overexpressed CENP-A (Lacoste et al., 2014; Shrestha et al., 2017a) and CIN phenotypes in HeLa cells (Shrestha et al., 2017a). We examined whether depletion of DAXX would suppress the higher invasion of DOX-treated DLD1^{CENP-A} cells. Western blot analysis confirmed the depletion of DAXX and showed that DAXX depletion does not affect the levels of YFP-CENP-A in DOX-treated DLD1^{CENP-A} cells (Fig. 6 D). We performed trans-well invasion assays as described above (Fig. 6 A) by using negative siRNA as control or DAXX siRNA-treated DLD1^{CENP-A} cells with or without DOX treatment. Quantification of the data showed that, upon DOX treatment, the number of invading cells in DAXX-depleted DLD1^{CENP-A} cells was significantly reduced compared with negative siRNA-treated DLD1^{CENP-A} cells (Fig. 6 E). In contrast, the number of invading cells was not significantly different in negative or DAXX siRNA-treated control DLD1^{CENP-A} cells compared with DAXX-depleted DLD1^{CENP-A} cells with DOX (Fig. 6 E). Taken together, our results show that CENP-A OE reduces the expression of cell adhesion genes and contributes to higher invasion of DLD1 cells. Our results further show that DAXX depletion rescues the CENP-A OE-induced higher invasion.

DLD1^{CENP-A} xenograft tumors with high expression of CENP-A are aneuploid and karyotypically heterogeneous

To examine how the physiological microenvironment would affect consequences due to CENP-A OE and to correlate the in vitro findings to an ex vivo set up, we developed a DLD1^{CENP-A} xenograft tumor model in nude mice. Ten mice were

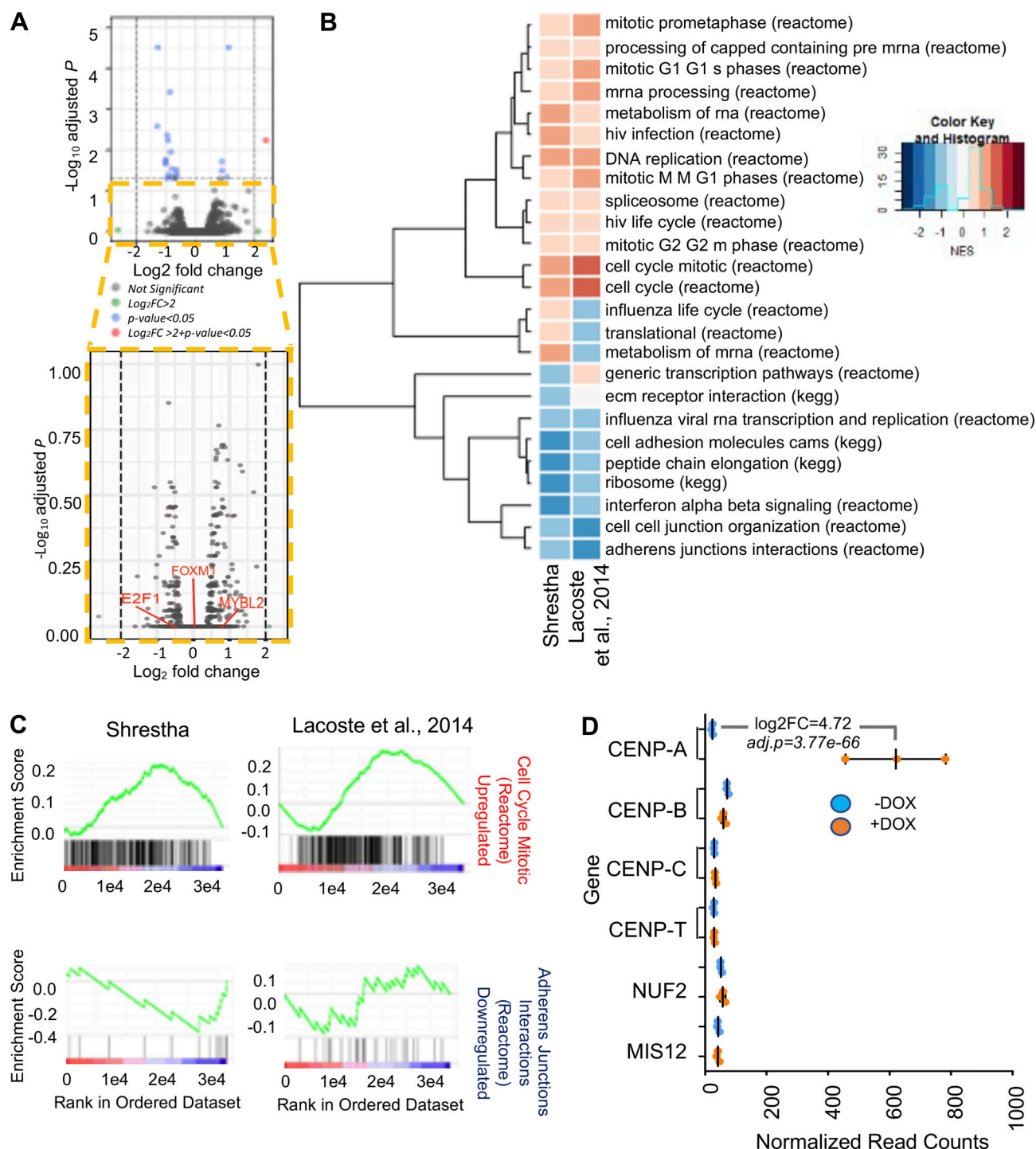


Figure 5. Reduced expression of cell adhesion genes in cells with CENP-A OE. (A) Volcano plot of \log_2 fold-change (\log_2FC) versus adjusted P value for gene expression changes in DLD1^{CENP-A} cells with DOX treatment over DLD1^{CENP-A} cells without DOX treatment. Area enclosed in yellow dashed line shows the spread of data with P value > 0.1 . (B) Heat map of GSEA normalized enrichment scores (NES) across two datasets. \log_2FC values of gene expression changes were used as input for GSEA of gene sets from Reactome and KEGG databases. Plot shows NES of terms significantly enriched in the dataset from this study (Shrestha) downregulated at FDR < 0.25 or upregulated at FDR < 0.005 and corresponding NES for same terms from Lacoste et al. (2014) with HeLa cells constitutively OE YFP-CENP-A data set. Line in color key represents density plot of NES scores across the two data sets. (C) GSEA enrichment plots for select terms enriched in Shrestha (current study) and Lacoste et al. (2014) data sets. Genes upregulated upon CENP-A OE, such as mitotic genes, are to the left (shaded red) and genes downregulated, such as adherens junction interactions, are to the right (shaded blue). Green line shows walking enrichment score. Black vertical bars represent hits from gene set. (D) Expression of candidate kinetochore genes are not upregulated in response to CENP-A OE. Normalized read counts generated by EdgeR for select CENP and kinetochore proteins. Error bars represent mean \pm SD. $\log_2FC < |0.28|$ and adjusted $P > 0.99$ for all genes shown, except CENP-A.

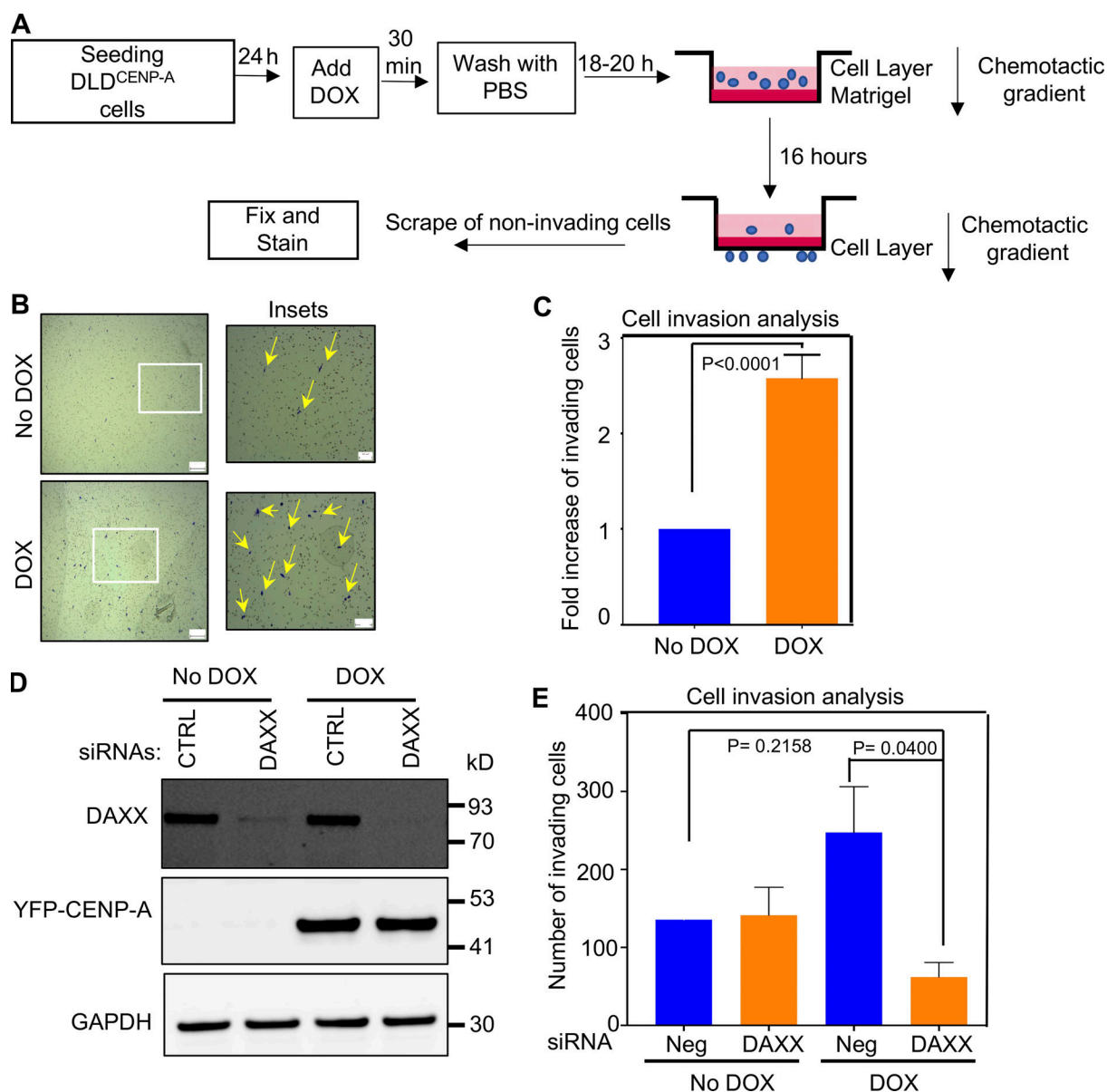


Figure 6. Higher invasion of cells with CENP-A OE. (A) Experimental regimen for invasion assay; see Materials and methods section for detail. (B) Higher invasion in DLD1 cells with overexpressed CENP-A. Images show the invasion of DLD1^{CENP-A} cells with or without DOX treatment across the trans-well membrane. Insets correspond to white-boxed areas in main images. Yellow arrows show invaded cells. (C) Quantification shows fold increase of invading DLD1^{CENP-A} cells treated as in D. Error bars represent the SD from four independent experiments. P values calculated by using unpaired Student's *t* test are indicated. (D) Depletion of histone chaperone DAXX suppresses the higher invasion in DLD1 cells with overexpressed CENP-A. Western blots show the protein levels of DAXX and YFP-CENP-A in cell lysates of DLD1^{CENP-A} cells with or without DOX treatment, followed by treatments with siRNA oligos as indicated. GAPDH was used as loading control. (E) Quantification shows the number of invading DLD1^{CENP-A} cells with or without DOX treatment, followed by treatments with siRNA oligos as indicated and calculated as in C. Error bars represent the SD from three independent experiments. P values calculated by using unpaired Student's *t* test are indicated. Ctrl, control.

subcutaneously (s.c.) injected with DLD1^{CENP-A} cells and fed with a control (CON) diet. Because DLD1 cells are colorectal cancer cells, tumors started appearing at day 9 in all 10 mice. Tumor volumes were regularly measured every 3–5 d. We observed exponential growth of tumors in all 10 mice fed with the CON diet. Once tumors reached an excisable volume after 16 d of s.c. injection, five mice were continued on the CON diet and the other five were fed with a DOX diet (200 mg/kg ad lib) to overexpress YFP-CENP-A. Interestingly, the growth of tumors in

mice on the DOX diet was slower than that in mice on the CON diet (Fig. 7 A). After 28 d, tumors were excised from a mouse from either the CON diet cohort (MDX#10) or DOX diet cohort (MDX#07). Tissue sections were prepared and analyzed by using immunohistochemistry (IHC) with a CENP-A antibody to examine CENP-A expression and with hematoxylin and eosin (H&E) staining for histological analysis. IHC examination confirmed that tumor tissues derived from MDX#7 had higher expression of CENP-A and higher incidence of CENP-A-positive

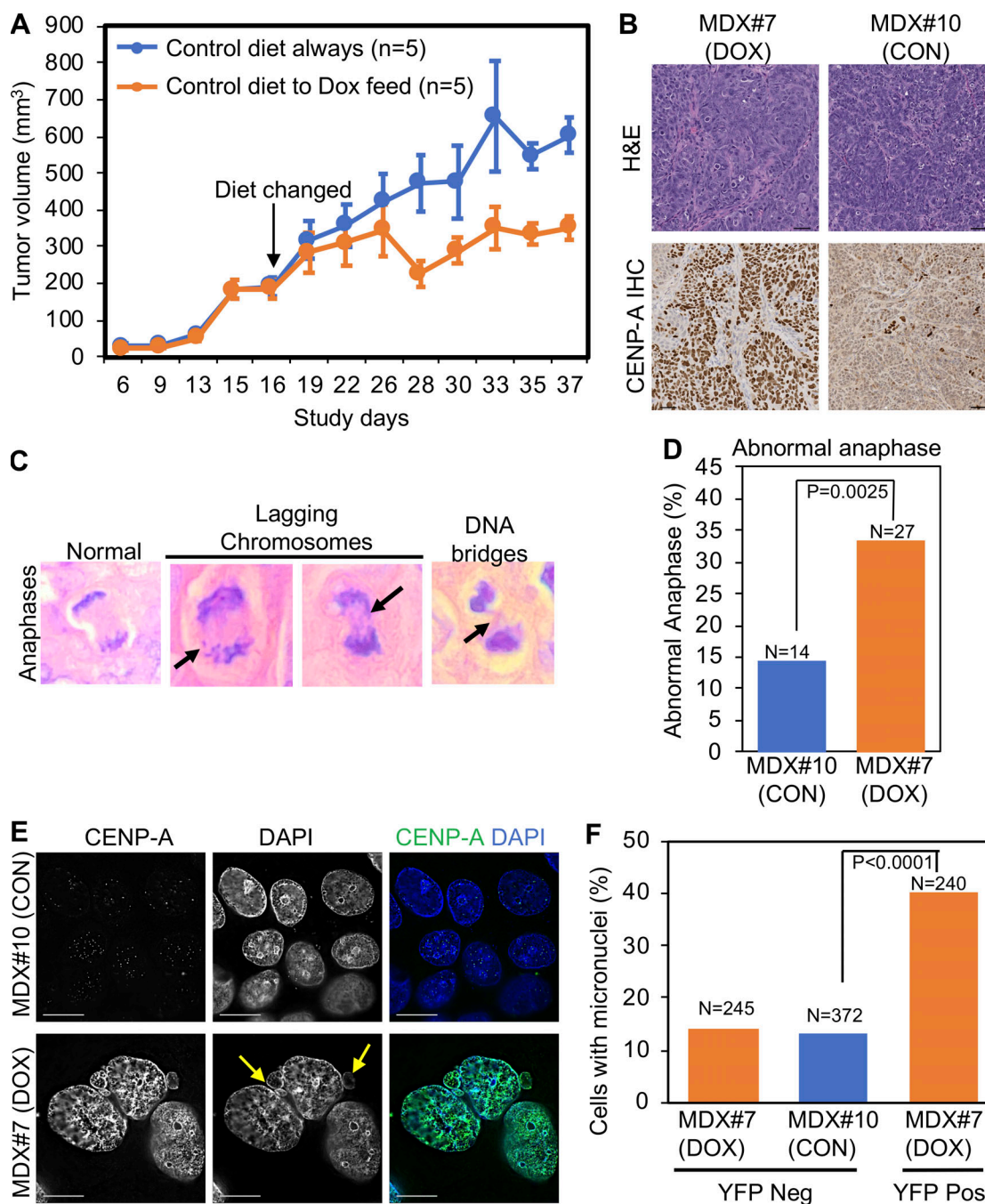


Figure 7. DLD1^{CENP-A} xenograft tumors with high expression of CENP-A exhibit abnormal mitoses and increased incidence of micronuclei. (A) Tumor volume in mice xenografted with DLD1^{CENP-A} cells and fed with CON or DOX diet. Ten mice that were s.c. injected with DLD1^{CENP-A} cells were fed with CON diet and tumor volumes were measured every 3–5 d. After 16 d of s.c. injection, five mice were continued on CON diet and the other five were fed with DOX diet (200 mg/kg ad lib) to overexpress YFP–CENP-A. Graph shows tumor volume in mm³ in mice fed with DOX diet (n = 5) or those that continued on CON diet (n = 5). (B) Higher expression of YFP–CENP-A in xenograft-induced tumor tissue of mouse fed on DOX diet. Images of IHC show YFP–CENP-A expression in tumor tissues of mice with DOX (MDX#07) or CON (MDX#10) diet. (C) Higher degree of abnormal mitoses in xenograft-induced tumor tissue of mouse on DOX diet. H&E-stained histological images show anaphases in tumors from mice with DOX (MDX#07) or CON (MDX#10) diet. Arrows in anaphase cells show abnormal anaphases as lagging chromosomes and DNA bridges. (D) Quantification of experiment (C) shows proportion of abnormal anaphases in H&E-stained tumor tissues from mice with DOX (MDX#07) or CON (MDX#10) diet. P value was calculated by using the χ^2 test. (E) Increased incidence of micronuclei in cells derived from xenograft-induced tumor from mouse fed with DOX diet. Images show micronuclei in cells derived from tumors of mice with DOX (MDX#07) or CON (MDX#10) diet. Cells were immunostained with antibodies against CENP-A, stained with DAPI, and analyzed for the presence of micronuclei in YFP-positive and -negative cells. Yellow arrows show micronuclei in cells derived from tumor of mouse fed on DOX diet. Scale bar: 5 μ m. (F) Quantification of experiment (E) shows the proportion of cells with micronuclei in cells derived as in C. “N” in D and F denotes the number of cells analyzed. P value was calculated by using the χ^2 test.

nuclei than tumor tissues derived from MDX#10 (Fig. 7 B and Fig. S5 A). Western blot analysis confirmed high levels of YFP-CENP-A in lysates prepared from tumor tissue of MDX#07 (Fig. S5 B). As expected, the lysates prepared from tumor tissue of MDX#10 did not show expression of YFP-CENP-A. Next, we examined evidence for CIN in DLD1^{CENP-A}-derived xenograft tumor tissues of MDX#10 or MDX#07. H&E-stained tissue sections were examined for abnormal mitoses, such as lagging chromosomes and DNA bridges (Fig. 7 C). Our results showed that tumor tissue from MDX#07 had significantly higher levels of abnormal anaphases—lagging chromosomes and DNA bridges—compared with tumor tissue derived from MDX#10 (Fig. 7 D).

We next generated single-cell suspension from xenograft tumors and determined the degree of CIN by quantifying the number of micronuclei in these cells. The analysis showed high expression of YFP-CENP-A in tumor-derived cells from MDX#07, but not from MDX#10 (Fig. 7 E), consistent with IHC staining and Western blot analysis of tumor tissues. The incidence of micronuclei in interphase cells without CENP-A OE (YFP negative) was lower in cells derived from tumors of MDX#07 and MDX#10 (Fig. 7, E and F). In contrast, YFP-CENP-A-positive tumor-derived cells from MDX#07 displayed significantly higher incidences of micronuclei (Fig. 7, E and F). The results for tissues and tumor-derived cells show that CENP-A OE contributes to CIN in the xenograft tumors.

The CIN phenotypes in CENP-A-overexpressing xenograft tumor tissues and in cells derived from these tissues prompted us to examine the karyotype of cells derived from xenograft tumor tissues. We used multiplex interphase FISH (miFISH) to enumerate the copy numbers of 10 gene-specific loci within each interphase nucleus, as previously described (Heselmeyer-Haddad et al., 2012). Two probe panels were designed targeting COX2 (1q31), BRAF (7q34), MYC (8q24), CDX2 (13q12), CDH1 (16q22), TP53 (17p13), SMAD4 (18q21), and ZNF217 (20q13), and centromeric probes—CEP3 and CEP10—were used as ploidy controls (Fig. 8 A). miFISH was performed on tumor-derived cells from MDX#7 and MDX#10 mice. To analyze the clonal composition in these cells, compared with its ploidy, we displayed each cell according to its gain (green), loss (red), or unchanged (blue) status (Fig. 8 B). Copy number alterations (CNAs) were higher in MDX#7 (40%) compared with MDX#10 (10%; Fig. 8 B). This is also depicted in a higher instability index (26.6) for MDX #7 compared with MDX#10 (7.1; Fig. 8 B and Table 1). DLD1 cells have a small population of tetraploid cells (Lengauer et al., 1997). When analyzing the diploid cell population for MDX#7 and MDX#10, cells with CNAs were 30.6% and 10%, respectively (Table 2). Likewise, in MDX#7 and MDX#10, the tetraploid cell populations consisting of cells with CNAs were 8.0% and 2.0%, respectively (Table 2). We did not observe a particular signature of karyotypic abnormality in the tumor-derived cell line from MDX#07; however, we did observe an enormous karyotypic heterogeneity with a mixture of gain or loss of multiple genes as shown by increased CNAs in the color chart (Fig. 8 B) for 33.6% of tumor tissue-derived cells from MDX#07 compared with only 10% of tissue-derived cells from MDX#10 (Fig. 8 B). Based on these results, we conclude that

CENP-A OE contributes to aneuploidy and karyotypic heterogeneity in DLD1^{CENP-A} xenograft tumors.

Constitutive high OE of CENP-A contributes to aneuploidy and karyotypic heterogeneity in DLD1 cells

We observed slow growth of CENP-A-overexpressing tumors in a xenograft model (Fig. 7 A) and aneuploidy with karyotypic heterogeneity in cells derived from CENP-A-overexpressing xenograft tumor (Fig. 8 B, Table 1, and Table 2). In the xenograft model, the mice were fed DOX diet continuously and YFP-CENP-A was constitutively overexpressed at high levels; therefore, we used a cell culture model to examine the consequences of constitutive high OE of CENP-A on cell viability and aneuploidy. We treated DLD1^{CENP-A} cells with 0.1 or 1.0 µg/ml DOX for 4 d to mimic constitutive high OE of YFP-CENP-A, as in the DLD1^{CENP-A} xenograft model, and examined its effects on cell viability and karyotype. Western blot analysis showed a dose-dependent increase in the levels of YFP-CENP-A in DLD1^{CENP-A} cells treated with different concentrations of DOX (Fig. S5 C). Immunofluorescence experiments confirmed high expression and mislocalization of YFP-CENP-A with 1.0 µg/ml DOX compared with those treated with 0.1 µg/ml DOX (Fig. S5 D). Brightfield microscopy images showed increased cell death in DLD1^{CENP-A} cells treated with 1.0 µg/ml DOX compared with those treated with 0.1 µg/ml DOX (Fig. S5 E). We quantified the total number and viability of DLD1^{CENP-A} cells treated with DOX (0.1 or 1.0 µg/ml) for 4 d. Both the total number of cells and cell viability were significantly reduced in DLD1^{CENP-A} cells treated with a higher concentration of DOX (1.0 µg/ml) for 4 d. These results show that constitutive high expression of CENP-A reduces cell proliferation and viability (Fig. S5 F). We next examined the effect of CENP-A OE on apoptosis-induced cell death by flow cytometry analysis with Annexin V and propidium iodide (PI) staining. A significant increase in apoptotic cells was observed in DLD1^{CENP-A} cells treated with a higher dose of DOX (1.0 µg/ml), but not in DLD1^{CENP-A} cells treated with the lower dose of DOX (0.1 µg/ml; Fig. S6, A and B). Control parental DLD1 cells treated with 0.1 or 1.0 µg/ml DOX did not show apoptotic cells (Fig. S6, A and B). Based on these results, we conclude that constitutive high OE of CENP-A contributes to reduced viability with apoptosis-induced cell death in DLD1 cells. We propose that increased apoptosis may have contributed to the initial slow growth of tumors in the xenograft mouse model.

Next, we used miFISH to examine the karyotype of cells constitutively expressing high levels of CENP-A. Since treatment of DLD1^{CENP-A} cells with 1.0 µg/ml DOX for 4 d showed massive apoptosis, we examined the karyotype in DLD1^{CENP-A} cells treated with 0.1 µg/ml DOX for 4 d. This analysis showed that 87% of DLD1^{CENP-A} cells without DOX treatment were diploid, with an instability index of 11.3% (Fig. 8 C and Table 1). In contrast, only 54% of DLD1^{CENP-A} cells with DOX treatment were diploid, with a higher instability index of 40% (Fig. 8 C and Table 1). Consistent with the results from our xenograft mouse model, we observed karyotypic heterogeneity in 42% of DLD1^{CENP-A} cells treated with DOX (Fig. 8 C and Table 2). Among the diploid cell population, proportions of aneuploid cells in DLD1^{CENP-A} cells without and with DOX treatment were 10.63%

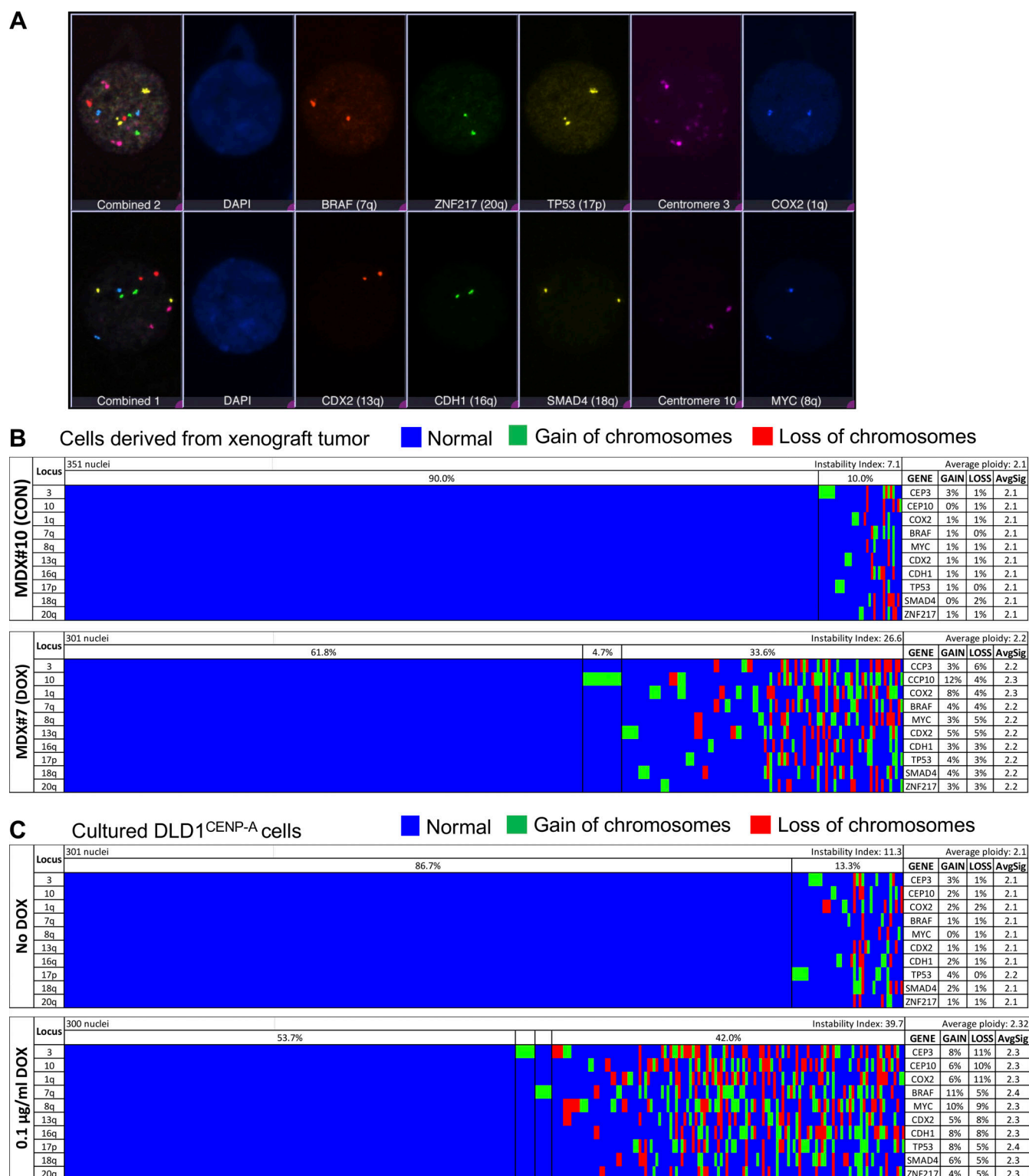


Figure 8. **Aneuploidy and karyotypic heterogeneity in cells derived from DLD1^{CENP-A} xenograft tumors and cultured DLD1^{CENP-A} cells with CENP-A OE.** (A) Probes used for miFISH experiments. Representative image of one cell hybridized with miFISH panels 1 and 2. The top row depicts the first hybridization, while the row underneath shows the second hybridization. The merged nuclei on the left of each row shows the overlay of all channels. (B) Cells derived from DLD1^{CENP-A} xenograft tumors exhibit aneuploidy and karyotypic heterogeneity. Color displays for miFISH with 10 probes depict increased aneuploidy and karyotypic heterogeneity in cells derived from xenograft-induced tumor from mouse fed with DOX (MDX#07) compared with CON (MDX#10) diet. (C) Constitutive CENP-A OE contribute to aneuploidy and karyotypic heterogeneity in cultured DLD1^{CENP-A} cells. miFISH analysis as in B of control DLD1^{CENP-A} cells or DLD1^{CENP-A} cells treated with 0.1 μ g/ml DOX for 4 d. DOX was replenished every 2 d for constitutive overexpression of YFP-CENP-A. The color scheme for each color display is as follows: green, gains; red, losses; and blue, unchanged, as determined by comparing each cell to the average ploidy. Nuclei are plotted vertically by pattern frequency. The gain and loss column refers to the percentage of nuclei where a gain or loss was observed with the 10 different probes.

Table 1. High instability index in cells derived from xenograft tumor and cultured DLD1CENP-A cells with constitutive CENP-A OE

Category	Instability index	
Cells derived from xenograft tumor tissues	MDX#10 (CON; <i>n</i> = 351)	MDX#7 (DOX; <i>n</i> = 301)
	7.1	26.6
Cultured DLD1 ^{CENP-A} cells	No DOX (<i>n</i> = 301)	DOX (<i>n</i> = 300)
	11.3	40

Quantification of instability indices from miFISH data acquired from Fig. 8 (B and C) in cells derived from xenograft tumors of mice fed with DOX (MDX#7) or CON diet (MDX#10) and from cultured DLD1^{CENP-A} cells with or without DOX treatment for 4 d.

and 31.0%, respectively (Table 2). Likewise, among the tetraploid cell population, proportions of aneuploid cells in DLD1^{CENP-A} cells without and with DOX treatment were 2.32% and 15.33%, respectively (Table 2). Based on these results, we conclude that constitutive OE of CENP-A contributes to aneuploidy with karyotypic heterogeneity in DLD1 cells. The increased apoptosis in cells with constitutively high OE of CENP-A suggest that the tumor regression in the DLD1^{CENP-A} xenograft tumor model may be due to apoptosis in CENP-A-overexpressing cells; however, the cells that are resistant to apoptosis survive and display karyotypic heterogeneity, as observed in the xenograft mouse model.

Discussion

CENP-A OE leads to its mislocalization to non-centromeric regions and CIN in yeast, flies, and human cells (Au et al., 2008; Choi et al., 2012; Heun et al., 2006; Ranjitkar et al., 2010; Hewawasam et al., 2010; Ohkuni et al., 2016; Van Hooser et al., 2001; Lacoste et al., 2014; Athwal et al., 2015; Shrestha et al., 2017a). OE of CENP-A has been observed in many cancers and has been linked to decreased survival, increased invasiveness, poor prognosis, adverse tumor properties, metastatic spread, and increased levels of genomic instability (Zhang et al., 2016; Sun et al., 2016; Li et al., 2011). Despite these observations, the molecular consequences of CENP-A OE on CIN and aneuploidy have not been defined. Here, we used the pseudodiploid colorectal cancer cell line DLD1 and a xenograft mouse model to examine the molecular consequences of CENP-A OE on CIN,

mechanisms that contribute to CIN, and changes in karyotype in these cells. Our results showed that CENP-A OE leads to mislocalization of CENP-A to non-centromeric regions and CIN in DLD1 cells and a xenograft mouse model. We determined that the CIN phenotypes, as assessed by chromosome segregation defects with higher incidence of lagging chromosomes and micronuclei in DLD1 cells, were due to defects in kinetochore integrity because of reduced protein levels at the kinetochore and unstable KT-MT attachments. Furthermore, we showed that CENP-A OE and mislocalization contribute to aneuploidy with karyotypic heterogeneity in both DLD1 cells and a xenograft mouse model. In summary, our studies provide mechanistic insights into how CENP-A OE and mislocalization lead to CIN, and provide the first link between CENP-A OE and aneuploidy with karyotypic heterogeneity.

Several studies have linked the formation of micronuclei with various chromosomal aberrations related to CIN, such as defective chromosome segregation, chromosome fragmentation, mitotic cell death, mitotic catastrophe, and double-stranded DNA breaks (Ye et al., 2019). Along with the increased incidence of micronuclei, we also observed increased lagging chromosomes in cells with CENP-A OE. During mitotic exit, lagging chromosomal fragments can recruit nuclear envelope components to form micronuclei that are compartmentally separated from the primary nucleus; however, it has been previously demonstrated that lagging chromosomes and micronuclei are prone to go through irreversible loss of compartmentalization due to defects in nuclear envelope assembly (Hatch et al., 2013; Liu et al., 2018). In line with these findings, we observed that the

Table 2. Aneuploidy with increased CNAs in cells derived from xenograft tumor and cultured DLD1CENP-A cells with constitutive CENP-A OE

Category	Ploidy	CNAs (%)		
Cells derived from xenograft tumor tissues		MDX#10 (CON; <i>n</i> = 351)	MDX#7 (DOX; <i>n</i> = 301)	P value
	Diploid	10	30.6	<0.00001
	Tetraploid	2	8	0.0003
Cultured DLD1 ^{CENP-A} cells		No DOX (<i>n</i> = 301)	DOX (<i>n</i> = 300)	P value
	Diploid	10.6	31	<0.00001
	Tetraploid	2.3	15.3	0.0026

Quantification of CNAs based on miFISH experiments from Fig. 8 (B and C) showing the proportion of diploid and tetraploid cells with CNA in cells derived from xenograft tumor from mice fed with DOX (MDX#7) or CON diet (MDX#10) or from cultured DLD1^{CENP-A} cells with or without DOX treatment for 4 d. P values were calculated by using Fisher's exact test in R laboratory.

majority of the micronuclei in CENP-A-overexpressing cells have ruptured nuclear membranes, as shown by partial Lamin B signal. Cells containing micronuclei with defective envelopes are prone to go through genomic rearrangements and chromothripsis (Zhang et al., 2015). Hence, it will be of interest to examine if CENP-A OE contributes to chromothripsis.

We used several independent assays to examine the molecular basis for the CIN phenotypes due to CENP-A OE. For example, we examined the localization of CENP-C and a subset of other centromeric and kinetochore proteins in CENP-A OE cells. Consistent with previous studies in HeLa and SW480 cells (Nye et al., 2018; Shrestha et al., 2017a; Van Hooser et al., 2001), we observed mislocalization of CENP-C, a component of the CCAN network that interacts with CENP-A (Kato et al., 2013; Falk et al., 2015), to non-centromeric regions in cells with CENP-A OE. Interestingly, centromeric recruitment of CENP-C was also reduced, suggesting that titration of CENP-C to non-centromeric regions may contribute to reduced levels at centromeres. We also observed reduced levels of CENP-T at centromeres in cells with CENP-A OE. CENP-T, another component of the CCAN network, is a constitutive DNA-binding protein that serves as a structural platform for outer kinetochore assembly by binding with Spc24/25 of the Ndc80 complex (Nishino et al., 2012). Depletion of CENP-T abolishes the structure of outer kinetochore and lowers the levels of the Ndc80 complex and contributes to chromosome segregation defects (Hori et al., 2008; Gascoigne et al., 2011; Suzuki et al., 2015). Consistent with a role for CENP-T in the recruitment of outer kinetochore proteins, we observed reduced levels of Ndc80 complex—NUF2 and HEC1—and Mis12 proteins at kinetochores in CENP-A-overexpressing cells. NUF2 and HEC1, the core components of the outer kinetochore plate, are essential for stable KT-MT attachments (DeLuca et al., 2005). The reduced levels of these proteins are not due to defects in the expression of the corresponding genes, as revealed by RNAseq analysis of DOX-treated DLD1 cells. Hence, we propose that mislocalization of CENP-A may titrate proteins, such as CENP-C, to ectopic sites and this, together with reduced levels of proteins, such as CENP-C, CENP-T, Ndc80, and Mis12 at kinetochores, leads to CIN.

To understand the molecular basis for the CIN phenotype in cells with CENP-A OE, we investigated the physiological consequences of reduced levels of proteins at kinetochores. This was done by examining interkinetochore distance, cold stability of microtubules, and status of KT-MT attachments. Interkinetochore distance between two sister KTs in cells with CENP-A OE was reduced, indicating that these cells have defects in kinetochore integrity. Reduced interkinetochore distance due to weakened endogenous kinetochores has been reported in cells depleted of NUF2 and in those with abrogation of the Ndc80 complex (Sundin et al., 2011). Our results for reduced localization of CENP-T, NUF2, HEC1, and Mis12 are consistent with defects in kinetochore integrity in cells with CENP-A OE. Previous studies have shown that loss of CENP-A methylation also weakens kinetochores through loss of CENP-T and CENP-I at centromeres, resulting in chromosome mis-segregation (Sathyan et al., 2017). Further support for defects in kinetochore integrity is derived from defects in KT-MT attachments

due to CENP-A OE. The status of KT-MT attachments was examined by using cold-resistant microtubule stability assays and KT localization of Astrin, a microtubule plus-end binding protein that is recruited to kinetochores once stable KT-MT attachments are made (Shrestha and Draviam, 2013). The density of microtubules that are stably attached to kinetochores in an end-on fashion and the levels of KT-associated Astrin were significantly lower in CENP-A-overexpressing cells. Our observations with cells overexpressing CENP-A are consistent with several studies that have shown a correlation between reduced levels of outer KT proteins, unstable KT-MT attachments, and chromosome segregation defects. For example, immunofluorescence and transmission EM approaches have shown that cells depleted of NUF2 and HEC1 show reduced levels of end-on KT-MT bundles and misaligned chromosomes (DeLuca et al., 2005). Another study by Dudka et al. (2018) showed that reduced KT-MT attachments contribute to reduced interkinetochore distance and chromosome segregation defects. Our results provide mechanistic insights into how reduced levels of outer kinetochore proteins and reduced KT-MT occupancy compromises kinetochore integrity, leading to CIN phenotypes in cells with CENP-A OE.

Bioinformatic studies have shown high levels of CENP-A mRNA in chromosomally unstable cancers (Zhang et al., 2016). To further define the consequences of CENP-A OE, we performed transcriptomic analysis and observed differential expression for certain gene categories in CENP-A-overexpressing DLD1 cells that was similar to that in HeLa cells with constitutive CENP-A OE (Lacoste et al., 2014). Both studies show an enrichment of genes related to mitosis in response to CENP-A OE. This may be due to the aneuploid nature of CENP-A-overexpressing cells and/or OE of mitotic genes reported in aneuploid and CIN cells (Carter et al., 2006; Pfister et al., 2018). As for genes that showed reduced expression upon CENP-A OE, we identified genes encoding for CAMs similar to those reported previously for HeLa cells with constitutive CENP-A OE (Lacoste et al., 2014). CAMs play a role in cancer invasion and metastasis, serving to promote invasion or suppress metastasis in epithelial tumor cells and lymph nodes (Behrens, 1993; Sulzer et al., 1998; Vleminckx et al., 1991; Makrilia et al., 2009). Consistent with these studies, we observed higher invasiveness of DLD1 cells with CENP-A OE. Increased cell invasiveness of DLD1 cells with CENP-A OE was similar to that observed in breast cancer cell lines with Ras suppressor-1 depletion or in DLD1 cells with Tet1 depletion (Gkretsi et al., 2019; Zhou et al., 2018). Depletion of histone chaperone DAXX rescued the higher invasion phenotype of CENP-A-overexpressing DLD1 cells. We and others have shown that the depletion of DAXX partially suppresses the mislocalization of overexpressed CENP-A in HeLa cells (Lacoste et al., 2014; Shrestha et al., 2017a). The level of mislocalization of CENP-A is much higher in DOX-treated DLD1^{CENP-A} cells compared with that observed in HeLa^{CENP-A} cells (Shrestha et al., 2017a). We were unable to discern suppression of CENP-A mislocalization after the depletion of DAXX in DOX-treated DLD1 cells. One possible explanation for these observations may be the highly saturated levels of mislocalized CENP-A in DOX-treated DLD1^{CENP-A} cells. Although we could not observe a change in

CENP-A mislocalization, DAXX suppression had no effect on cell invasion in the absence of CENP-A OE, showing that the effect of DAXX is through its effect due to overexpressed CENP-A and not through effects on H3.3 or other DAXX function.

Based on our results, for rescue of higher invasiveness of DLD1 cells with CENP-A OE, we propose that DAXX depletion may have a distinct advantage to prevent invasiveness resulting from CENP-A OE. Several observations support this proposal because mutations or deletion in DAXX predict better prognosis of tumors (de Wilde et al., 2012; Pan et al., 2013b; Pan et al., 2013a), and high levels of DAXX are observed in metastatic pancreatic cancer (Puto et al., 2015). High invasion correlates with metastasis of tumors and is consistent with increased expression of CIN-associated genes in metastatic tumors than in primary tumors (Carter et al., 2006). It will be of interest to examine if CENP-A OE contributes to increased invasiveness of cells in animal models and human cancers.

We extended our studies by examining the consequences of CENP-A OE on its localization, CIN, and karyotype in a DLD1^{CENP-A} xenograft mouse model. Our results showed that CENP-A-overexpressing tumor tissues exhibit increased expression of CENP-A, higher incidence of CENP-A positive nuclei, and CIN phenotypes, such as micronuclei, lagging chromosomes and DNA bridges. Most importantly, cells derived from CENP-A overexpressing tumor tissues showed significantly higher levels of CNAs, with higher instability indices and increased karyotypic heterogeneity. These results are consistent with the consequences of CENP-A OE in cultured DLD1 cells. Interestingly, xenograft tumors with CENP-A OE showed initial slow tumor growth. We hypothesized that aneuploidy may have contributed to apoptosis and initial slow tumor growth in the xenograft tumor model. Previous studies have shown that chromosomal imbalances or aneuploidy generate proteotoxic stress with detrimental effects on cellular fitness, cell-cycle arrest, or apoptosis (Zhu et al., 2018; Siegel and Amon, 2012); however, immunofluorescence and histological examination of tissues and cells did not show a significant increase in mitotically arrested cells. Consistent with our hypothesis, constitutive high OE of CENP-A showed massive loss of cell viability and apoptosis-induced cell death in DLD1 cells. Based on our results from cell line and a xenograft mouse model, we propose that CENP-A-overexpressing tumor cells that are resistant to apoptosis survive and these cells exhibit aneuploidy with karyotypic heterogeneity.

In summary, our studies provide mechanistic insights into how CENP-A OE and mislocalization lead to CIN, and provide the first link between CENP-A OE and aneuploidy with karyotypic heterogeneity. Based on our results, we propose a model (Fig. 9) in which CENP-A OE and mislocalization contribute to (1) CIN phenotype with chromosome mis-segregation and increased micronuclei with ruptured nuclear membrane; (2) mislocalization of CENP-C, reduced levels of CCAN proteins (CENP-C and/or CENP-T) and outer kinetochore proteins (Mis12, NUF2, and HEC1), unstable KT-MT attachments, and weakening of kinetochores as ascertained by reduced interkinetochore distance; and (3) aneuploidy and karyotypic heterogeneity in cell line and a xenograft mouse model. These studies are important from a clinical standpoint as bioinformatics approaches have shown

that tumors with high expression of 14 kinetochore genes, including CENP-A, are associated with adverse tumor properties and predict poor patient outcome, metastatic spread, reduced survival, and increased levels of genomic instability in many cancer types (Zhang et al., 2016). Furthermore, CENP-A OE has been shown to correlate with cancer progression and poor prognosis in 20 different cancers, including colorectal, prostate, lung, and breast cancers (Zhang et al., 2016). Our studies suggest that aneuploidy with karyotypic heterogeneity may contribute to the aggressive phenotype of CENP-A-overexpressing cancers.

Materials and methods

Cell culture and generation of DLD1^{CENP-A} cell line

All cell lines were cultured at 37°C with 5% CO₂ supply in corresponding media supplemented with 10% FCS (F6178; 500 ml; Sigma-Aldrich), penicillin/streptomycin (15140122), fungizone (15290018), and L-glutamine (A2916801). The DLD1 cell line was cultured in RPMI 1640 medium (12633020; Thermo Fisher Scientific), the RPE1 cell line was cultured in DMEM:F12 medium (11330057; Thermo Fisher Scientific), and other cell lines—HeLa, HEK293T, and MDA-MB-231—were cultured in DMEM medium (12291023; Thermo Fisher Scientific). Stock cells were mixed in freezing media (medium with 50% FCS and 5% DMSO [85190]) and stored at -80°C. All reagents were purchased from Thermo Fisher Scientific unless otherwise stated. For DOX induction, cells were treated with the stated concentrations of DOX (D3447; 500 mg; Sigma-Aldrich) for 30 min, followed by three washes with PBS with 5-min intermittent incubation at 37°C and continued growth in DOX-free media for at least 20 h unless otherwise stated.

CENP-A targeting in the DLD1 cell line was made by using Transcription activator-like effector nucleases as previously described (Hoffmann et al., 2016). mCherry-H2B was cloned into a pSMPUW-based vector for lentivirus generation, and positive cells were isolated by using FACS technique (FACS Aria; BD Biosciences). EYFP-CENP-A was cloned into a pcDNA5/FRT/TO-based vector (Invitrogen), and stably integrated clones were selected with 400 µg/ml hygromycin (10-687-010; Gibco).

Chromosome spread preparation

For CENP-A localization studies, chromosome spreads were prepared as previously described (Shrestha et al., 2017a). Briefly, cells were treated with 0.1 µg/ml colcemid (10295892001; Roche) for 4–6 h, followed by mitotic shake off. Mitotic cells were then treated with hypotonic solution, 0.8% sodium citrate, and incubated at 37°C for 20 min; cells were centrifuged at 1,200 rpm for 5 min, and the supernatant removed. The cell pellet was mixed with 0.8% sodium citrate, and an appropriate volume of mixed cells was added into the cytospin funnel and spun at 900 rpm for 5 min. Slides containing cells were dipped in coplin jar with 4% PFA for 20 min at RT for fixation, followed by permeabilization with 0.1% Triton X-100 (X100-100ML; Sigma-Aldrich) for 10 min at RT. Cells were then washed with PBS + 0.1% Tween 20 (PBST; P9416-199ML; Sigma-Aldrich) three times for 5 min each, followed by incubation with 1% BSA + PBST for 30 min at RT. Cells were then incubated with

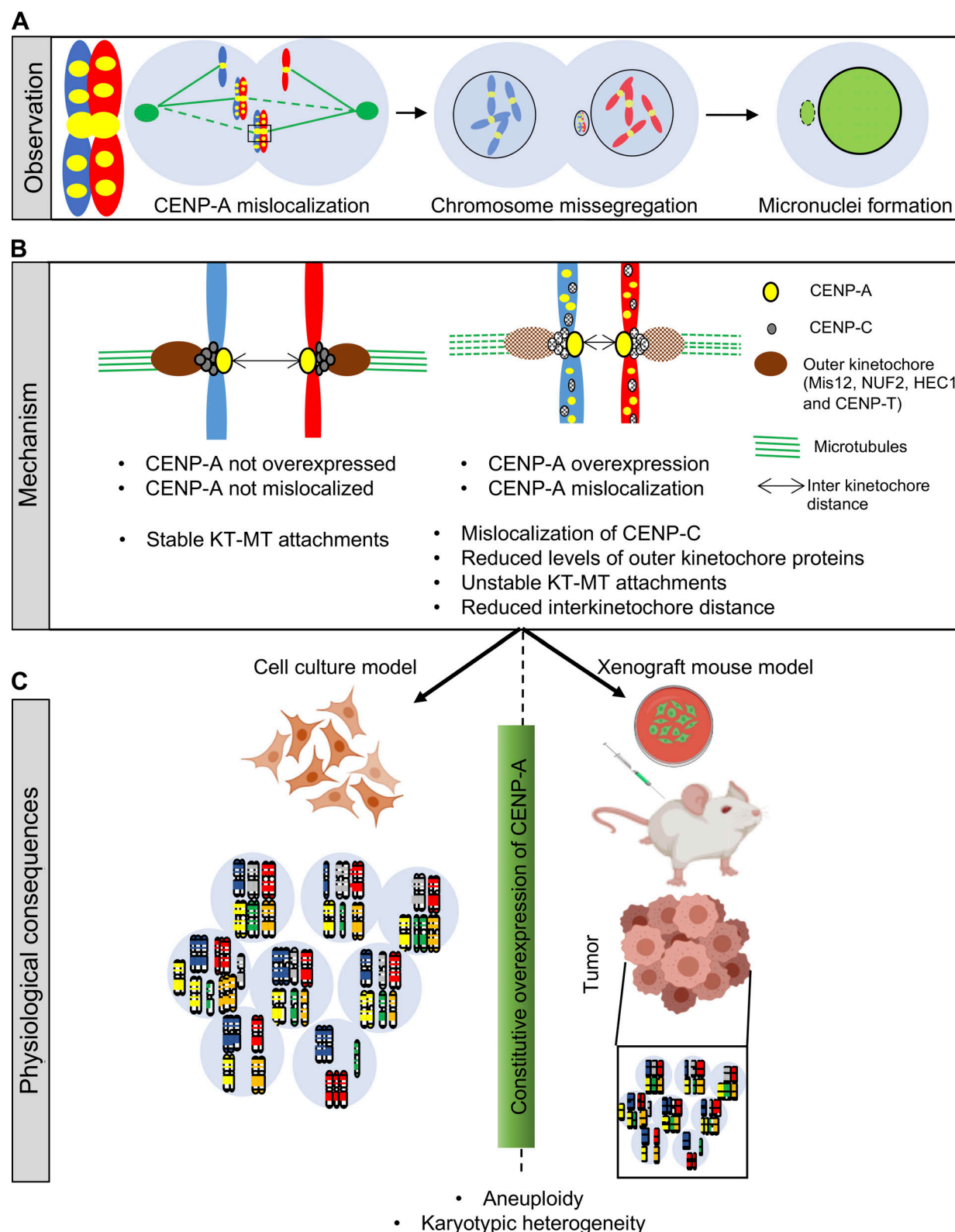


Figure 9. **CENP-A OE and mislocalization contribute to CIN, aneuploidy, and karyotypic heterogeneity in cell line and a xenograft mouse model.** (A) Observation: Mislocalization of CENP-A contributes to CIN phenotypes, chromosome mis-segregation, and micronuclei formation with ruptured nuclear membrane. (B) Mechanism: In control cells (left) without CENP-A OE and mislocalization, the levels of kinetochore- and centromere-associated proteins are normal, with normal pulling force between two sister kinetochores; however, cells with CENP-A OE and mislocalization (right) show mislocalization of CENP-C, reduced levels of outer kinetochore proteins (CENP-T, NUF2, HEC1, and Mis12), resulting in unstable KT-MT attachments and reduced interkinetochore distance. (C) Physiological consequences: Constitutive OE of CENP-A contributes to aneuploidy and karyotypic heterogeneity in cell line and a xenograft tumor model.

appropriate primary and secondary antibodies at RT for 1 h. Cells were then analyzed by immunofluorescence.

Immunostaining and immunoblotting

For immunostaining, cells were grown on glass coverslips and fixed either with ice-cold methanol for 1 min or with 4% PFA for 5 min, followed by permeabilization with 0.1% Triton X-100 for 5 min. Fixation was followed by blocking with 1% BSA in PBST for 30 min at RT. Cells were incubated in primary antibodies for 1 h at RT, washed three times in PBST, and incubated with secondary antibodies and DAPI for 45 min at RT. Following three washes with PBST, cells were mounted on slides by using Pro-long gold antifade mounting media (P36935; Thermo Fisher Scientific). Mouse anti-CENP-A (ab13939; Abcam), rabbit anti-NUF2 (ab176556; Abcam), rabbit anti-Astrin (NB100-74638; Novus Biologicals), mouse anti-HEC1 (MA1-23308; Thermo Fisher Scientific), rabbit anti-Mis12 (gift from Ian Cheeseman, Massachusetts Institute of Technology, Cambridge, MA), rabbit anti-CENP-T (gift from Daniel Foltz, Northwestern University, Evanston, IL), and rabbit anti-CENP-C (gift from Aaron Straight, Stanford University, Stanford, CA) were used at 1:500 dilutions. Rabbit anti-Lamin B antibody (gift by Mary Dasso, National Institute of Child Health and Human Development/National Institutes of Health, Bethesda, MD) was used at 1:2,000 dilution. Mouse anti-tubulin (T4026; Sigma-Aldrich) was used at 1:1,000 dilution. The secondary antibodies, goat anti-rabbit DY 488 (35552; Thermo Fisher Scientific), goat anti-rabbit DY 594 (35560; Thermo Fisher Scientific), goat anti-mouse DY 488 (35502; Thermo Fisher Scientific), goat anti-mouse DY 594 (35510; Thermo Fisher Scientific), and goat anti-human Alexa Fluor 647 (A21445; Thermo Fisher Scientific) were used at 1:500 dilution.

For immunoblotting, mouse anti-CENP-A (ab13939; Abcam) was used at 1:300 dilution. Rabbit anti-DAXX (25C12; Cell Signaling Technology) and rabbit anti-GFP antibody (ab6556; Abcam) were used at 1:1,000 dilution. Mouse anti-GAPDH (MA5-15738; Thermo Fisher Scientific) was used at 1:2,000 dilution. HRP secondary antibodies against rabbit (611-1322; Rockland) and mouse (610-1319; Rockland) were used at 1:40,000 dilution. Blots were treated with uniglow reagent (Uniglow-0100; Rockland) before imaging with Bio-Rad Imager. Bands were compared against the prestained protein ladder (MEIP8-501; Vita Scientific).

Microscopy and image analysis

Immunostained cells were imaged on Delta Vision Core system (Applied Precision/GE Healthcare) consisting of an Olympus IX70 inverted microscope (Olympus America) with 100× NA 1.4 oil immersion objective and a CoolSnap HQ 12-bit camera (Photometrics) controlled by Softworx software. Filters used for imaging were FITC (Ex 490/20; Em 528/38), RD-TR (Ex 555/28; Em 617/73), and DAPI (Ex 360/40; Em 457/50) from the 86000 Sedat Quadruple Filter Set (Chroma Technology). Z-stacks of at least 10 focal planes were acquired with an exposure of 0.1–0.5 s, depending on the filter. Signal intensity was measured by using the plot profile tool in Softworx. To prepare the figures, images were deconvolved, unless otherwise mentioned, with Softworx

and scaled manually to 8 bit by using linear LUT and the same range of scaling for all the images. For time-lapse imaging, cells were grown on a glass-bottom imaging dish, Nunc Lab Tek (155382; Thermo Fisher Scientific) in appropriate media. While imaging, Leobovitz (L-15; 21083027; Thermo Fisher Scientific) media was used. Cells were imaged with FITC (Ex 490/20; Em 528/38) and differential interference contrast (DIC) with exposure of 50% for 0.2 s. Cells were imaged at the time interval of 10 min for 5 h.

Quantitative immunofluorescence analysis

To calculate fluorescence intensities, boxes of 8×8 pixels were drawn on centromeric or kinetochore regions, as ascertained by foci of CENP-A, as well as on non-centromeric regions, as ascertained by the signal outside the centromeric region on a chromosome (chromosome spreads) or chromosomes aligned on the metaphase plate. Nondeconvolved images were used for fluorescence intensity measurement. For background, four boxes of 8×8 pixels were drawn at four random areas within the cytoplasm in the same cell. The maximum intensity values from all drawn areas were obtained by using the data inspector tool in Softworx. Final fluorescence intensity for each protein was calculated by subtracting the average background intensity. Intensity measurements were done for at least 10 centromeric and non-centromeric spots in each cell for an average of 10 cells from two or three independent experiments. Nondeconvolved images were used for fluorescence intensity measurement. For statistical analysis, average values from more than 100 centromeric or non-centromeric spots were calculated and used as a mean to calculate SD across areas measured.

Cell proliferation assay using EdU

Cells were treated with 20 μ M EdU for 30 min. 0.5×10^6 cells per sample were harvested by centrifugation and cell pellets were fixed with 100 μ l of 4% PFA for 15 min at RT, washed, and blocked with PBS with 5% BSA. Cells were then permeabilized with 100 μ l of 0.5% Triton X-100 with 5% BSA in PBS for 30 min at RT. 3 ml PBS with 1% BSA was added, and cells were centrifuged and washed once. Appropriate volume of Click-iT reaction cocktail was prepared according to the manufacturer's instructions (C10269; Thermo Fisher Scientific). 250 μ l of reaction cocktail buffer was added to each sample, mixed, and incubated for 30 min at RT. 3 ml PBS with 1% BSA was added to each sample, centrifuged, and washed. Cells were then suspended in 0.5 ml PBS with 2 μ g/ml DAPI and analyzed in a flow cytometer.

Cell viability assay

The trypan blue dye exclusion test was used to determine the number of viable cells present in a cell suspension. It is based on the principle that live cells with intact cell membranes exclude trypan blue, whereas dead cells do not and thus stain blue. Cells were harvested and 10 μ l of harvested cells were mixed with 10 μ l of 0.4% trypan blue dye (T13001; Logos Biosystem). The mixture was incubated for 3 min at RT. 10 μ l of the cell-dye mixture was then pipetted into the disposable counting chamber (L12005; Logos Biosystem), allowing the capillary action to draw

it inside. The total number of cells and viable cells were counted by using an automated cell counter (LUNA Automated Cell Counter).

Interkinetochore distance measurement

Interkinetochore distance was measured by using the distance measurement tool in Softworx, which allows a straight line to be drawn between the brightest pixels of CENP-A (inner kinetochore marker) or NUF2 (outer kinetochore marker) on two sister chromatids. Only congressed pairs of kinetochores in MG132 arrested metaphase cells were included for analysis to exclude any chromosomes that were not aligned, as in prometaphase, or nearly separated, as in anaphase, with reduced or increased interkinetochore distance, respectively. Orientation between two centromeric/kinetochore markers and focal plane was used as a basis for considering two kinetochores a pair. We used the following criteria to consider two kinetochores a pair in a cell immunostained with NUF2 and CENP-A: (1) Both kinetochores should be on the same focal plane; (2) kinetochores should be positive for NUF2 and CENP-A signals, with colocalization of both proteins; (3) because NUF2 localizes to the outer kinetochore where microtubules attach, NUF2 signal of both sister kinetochores should orient toward the spindle pole from where the microtubules emanate; and (4) because CENP-A localizes at inner centromere proximal to DNA, CENP-A signal of both sister kinetochores should orient toward the equatorial plate. The length of each line is calibrated based on units per pixel and assigned in micrometers. Interkinetochore distance was measured for at least 10 kinetochore pairs in a single cell and 8–15 cells from two or three independent experiments. Average values from more than 100 kinetochore pairs were calculated and used as the mean to calculate the SEM across areas measured.

KT-MT attachment status analysis

To define the KT-MT attachment status, we used NUF2 as the outer kinetochore marker and tubulin as the microtubule marker. We included only those cells in which more than 60% of KT-MT attachment status could be assigned. KT-MT attachments were assigned as end-on if the signals of tubulin in the microtubule bundles ended with NUF2. We categorized unattached and laterally attached kinetochores as non-end-on. KT-MT attachments were assigned as unattached if the NUF2 signal was free of tubulin signal, and laterally attached if NUF2 signal was on top of the tubulin signal of microtubule bundles.

Cold-resistant stable microtubule assay

Cells with or without DOX treatment were treated with 10 μ M dimethylenastron for 1.5 h, followed by treatment with 10 μ M dimethylenastron (324622-5MG; Sigma-Aldrich), an Eg5 inhibitor, and 10 μ M MG132 (474790-5MG; Sigma-Aldrich) for an additional 1.5 h. Culture dishes with cells containing coverslips were kept on ice for 10 min to depolymerize unstable microtubules. Cells were then immunostained with anti- β -tubulin and NUF2 or HEC1 and Astrin to examine the stable attachments between kinetochores and microtubules.

Trans-well invasion and apoptosis assay

Cells were seeded in a six-well dish for an arbitrary number of cells. 100 μ l of matrigel (356234; Corning) was added to the well of the trans-well containing 8.0 μ m transparent PET membrane (353182; Corning) and incubated at 37°C for 1 h. Trans-well was placed on the 12-well plate containing 1 ml RPMI supplemented with 20% FCS that served as a chemoattractant. 1 ml of 1.5×10^5 cells was added on top of the matrigel membrane and allowed to migrate for 16 h. The next day, cells on the matrigel membrane were scraped off from the membrane by using a sterile applicator and washed in PBS. This was repeated twice to make sure that all non-invading cells were scraped off. The cells that invade the membrane were fixed in ice-cold methanol for 10 min at 4°C, followed by two washes with PBS. Following fixation, cells were stained with crystal violet (0.05% in 25% methanol-PBS mixture) for 10 min to visualize through a microscope. The number of crystal violet-positive cells under the membrane were then counted and reported as invaded cells.

For the apoptosis assay, cells were harvested from suspension culture and stained with FITC Annexin V (556547; BD Biosciences) and PI (P4170; Sigma-Aldrich) by using the manufacturer's recommended protocol. FACS analyses were performed by using a dual-laser FACSscan (BD Biosciences).

siRNA

All siRNA transfections were performed by using Lipofectamine RNAi Max reagent (13778075; Thermo Fisher Scientific) according to the manufacturer's instructions. For RNAi, siRNA oligos and transfecting reagent were diluted in Opti-MEM reduced serum media (31985088; Thermo Fisher Scientific). siRNA oligo against DAXX (5'-CTGGAACCTGGCAAACAGAT-3') was ordered from Dharmacon (Shrestha et al., 2017a). For control siRNA, negative control oligo (12935-300; Invitrogen) was used.

miFISH

miFISH experiments were done as previously described (Oltmann et al., 2018). Probes were assembled from bacterial artificial chromosome contigs for the following eight locus-specific probes: COX2 (1q31), BRAF (7q34), MYC (8q24), CDX2 (13q12), CDH1 (16q22), TP53 (17p13), SMAD4 (18q21), and ZNF217 (20q13). Two centromeric probes—CEP3 and CEP10—were used as ploidy controls. The probes were combined into two FISH panels (panel 1: CDX2-CDH1-SMAD4-CCP10-MYC; panel 2: BRAF-ZNF217-TP53-CEP3-COX2). The panels were consecutively hybridized so that all 10 probes could be enumerated in each nucleus. Cells were fixed with methanol/acetic acid (3:1) before being dropped onto slides. A standard FISH hybridization and detection protocol was followed as described previously (Oltmann et al., 2018; <https://ccr.cancer.gov/Genetics-Branch/thomas-ried/under-resources>). After detection, the slides were automatically imaged with a fluorescence microscope equipped with a 40 \times oil immersion objective (BX63; Olympus), optical filters (Chroma Technology), motorized stage, and a custom analysis software (Bioview). Using the analysis software (Bioview), we counted ~300 cells in each case with 10 FISH probes presented in a custom gallery overview.

Xenograft mouse model

Athymic nude mice (female, 9-wk-old) were obtained from Charles River. Animals were injected with 5 million cells into the left flank with a 25-G needle in a volume of 100 μ l in HBSS as follows. The animals were placed on CON diet (Bioserv) ad lib ($n = 10$ animals) starting 2 d before cell injections. On day 15 post-cell injections, the animals were randomized into groups based on tumor volume and body weights by using StudyLog software. Five animals from the CON diet group were switched to 200 mg/kg DOX feed and five remained on the CON diet until the end of the study. The three axes (millimeters) of tumor were measured with a caliper to calculate tumor volume. Measurements were made every 2–3 d. Maximum allowable weight loss of 20% was never reached and mice were euthanized if tumor was presenting necrosis or exceeded 20 mm in diameter. Once the tumors were excised, they were used for single-cell suspension culture and histological investigation. For histological investigations, tumors were fixed in 10% neutral buffer formaldehyde (NBF), followed by preparation of thin sections and staining with H&E, or proceeded for IHC with anti-CENP-A Antibody. The H&E-stained tissues were used for examining abnormal mitoses, and IHC tissues were used to study levels of CENP-A. H&E and IHC slides were scanned at 20 \times by using an Aperio AT2 scanner (Leica Biosystems) into whole-slide digital images. For CENP-A IHC analysis, image analysis was performed by using Nuclear V9 algorithm in ImageScope version 12.4. Slides were annotated manually and areas of artifact, such as folds and tears, were excluded from analysis. Percent positive cells were calculated automatically. For cell CIN assays, single-cell suspension from tissues were prepared and cells were cultured for 48 h in complete DMEM media and used for examining protein levels of CENP-A, the incidence of micronuclei, and karyotype.

Xenograft mouse model studies were performed at Frederick National Laboratory, which is accredited by the Association For Assessment And Accreditation Of Laboratory Animal Care International and follows the Public Health Service Policy for the Care and Use of Laboratory Animals. Animal care was provided in accordance with the procedures outlined in the National Research Council's Guide for Care and Use of Laboratory Animals. All animal studies were approved by the Animal Care and Use Committee of the National Cancer Institute-Frederick.

Transcriptomic analysis

Parental DLD1 and DLD1^{CENP-A} cells with or without DOX were harvested from three independent biological replicates. RNA was isolated from cells with the RNeasy Plus Mini Kit (74134; Qiagen) according to manufacturer protocol. RNA quality and concentration were validated on a Bioanalyzer with the Agilent RNA 6000 Nano Kit (5067-1511; Agilent Technologies). 1 μ g of total RNA was used as input for RNaseq libraries, prepared according to the Low Sample protocol for Illumina TruSeq Stranded Total RNA Preparation Kit with Ribo-Depletion (RS-122-2201; Illumina). RNaseq libraries were single-end sequenced with the NextSeq 550 Sequencing System to a depth of \sim 90 million reads per sample. Raw BCL output files were processed by using bclfastq (version 2.17.1.14; Illumina) and quality

trimmed with trimmomatic (Bolger et al., 2014). Trimmed reads were aligned to the human genome (UCSC hg19) with TopHat (version 2.1.0; Trapnell et al., 2009) with gene annotations sourced from Ensembl release 72 assigned using Phython package HTSeq 0.6.1 (Anders et al., 2015). Differential gene expression was calculated by using EdgeR. RNaseq data sets from Lacoste et al. (2014) were downloaded from the Sequence Read Archive at the National Center for Biotechnology Information (accession nos. SRX297971–SRX297976). GSEA preranked analysis was performed with GSEA 3.0 (Broad Institute) by using log2FC values output from EdgeR (data set generated by this study and Lacoste data sets) against the Hallmarks: Canonical Pathways gene sets (c2.cp.v6.2.symbols.gmt; Subramanian et al., 2005). CENP-A expression values were omitted from ranked list input. Terms enriched in downregulated genes at false discovery rate (FDR) < 0.25 or enriched in upregulated genes at FDR < 0.005 from the DLD1 cell line data set from this study were analyzed further. Plots were generated in Rstudio.

Statistical analysis

P values were obtained by using either the Mann-Whitney U test, unpaired Student's *t* test, χ^2 test, or proportion test in Prism and Rstudio, as indicated in the figure legends.

Data and code availability

RNaseq data generated for this study has been deposited in the Gene Expression Omnibus under accession no. GSE154460.

Online supplemental material

Fig. S1 shows the optimization of DOX treatment to obtain the highest protein levels of YFP-CENP-A upon treatment with DOX. Fig. S2 shows the cell-cycle progression of DLD1 cells upon DOX treatment and rules out the effect of DOX alone in chromosome segregation defects in parental DLD1 cells. Fig. S3 shows the levels of CENP-T, Nuf2, and Mis12 at kinetochores in DLD1 cells with or without DOX treatment. Fig. S4 shows the KT-MT attachments and quantifies the localization of HEC1 and Astrin at kinetochores. Fig. S5 documents overexpression of CENP-A in xenograft tumor tissues and in cells derived from these tissues. Fig. S6 confirms that constitutive OE of CENP-A induces apoptosis in DLD1 cells. Video 1 shows a representative example of DLD1 cells with CENP-A OE exiting mitosis with chromosome segregation defects. Video 2 shows a representative example of DLD1 cells with CENP-A OE exiting mitosis and formation of micronuclei. Video 3 shows a representative example of a 3D-reconstructed image of DLD1 cells without CENP-A OE showing Astrin-positive kinetochores. Video 4 shows a representative example of a 3D-reconstructed image of DLD1 cells with CENP-A OE showing kinetochores devoid of Astrin.

Acknowledgments

We are grateful to Aaron Straight, Mary Dasso, and Iain Cheeseman for the generous gift of antibodies; Kajal Biswas and Shyam Sharan for tissue culture facility at the National Cancer Institute, Frederick, MD, for xenograft experiments; Mirit Aladjem and Haiquing Fu for assistance with cell proliferation

assays; and Mary Dasso, Anna Roschke, and members of the Basrai laboratory for discussions and comments on the manuscript. The content of this publication does not necessarily reflect the views or policies of the U.S. Department of Health and Human Services, nor does mention of trade names, commercial products, or organizations imply endorsement by the U.S. Government.

This work was supported by the Intramural Research Program of the National Institutes of Health, National Cancer Institute. D.R. Foltz and A.K. Hogan were supported by National Institutes of Health grant R01GM111907 and a Zell Scholar award from the Robert H. Lurie Comprehensive Cancer Center. D. Fachinetti was supported by the Centre National de la Recherche Scientifique. C.L. Sanders, S. Difilippantonio, and B. Karim were funded by the National Institutes of Health, National Cancer Institute, under contract no. 75N91019D00024.

The authors declare no competing financial interests.

Author contributions: Experiments were designed and conceived by R.L. Shrestha and M.A. Basrai. Figure contributions: A. Rossi (Fig. 1, A and B; Fig. 2, A and B; Fig. 4, A and B; Fig. 6, A–E); K.S. Zaldana (Fig. S2, C and D; and Fig. 8 C); E. Suva (Fig. S2, C and D); D. Wangsa and T. Ried (Fig. 8, Table 1, and Table 2); Y.J. Chung and P.D. Aplan (Fig. S6, A and B); C.L. Sanders, S. Difilippantonio, and B. Karim (Fig. 7, A–C); and A.K. Hogan and D.R. Foltz (Fig. 5). T.S. Karpova provided technical advice for microscopic analysis, and D. Fachinetti provided cell lines. Manuscript was written by R.L. Shrestha and M.A. Basrai. All the authors read and agreed on the publication of this manuscript.

Submitted: 30 July 2020

Revised: 15 December 2020

Accepted: 26 January 2021

References

- Anders, S., P.T. Pyl, and W. Huber. 2015. HTSeq—a Python framework to work with high-throughput sequencing data. *Bioinformatics*. 31:166–169. <https://doi.org/10.1093/bioinformatics/btu638>
- Athwal, R.K., M.P. Walkiewicz, S. Baek, S. Fu, M. Bui, J. Camps, T. Ried, M.H. Sung, and Y. Dalal. 2015. CENP-A nucleosomes localize to transcription factor hotspots and subtelomeric sites in human cancer cells. *Epigenetics Chromatin*. 8:2. <https://doi.org/10.1186/1756-8935-8-2>
- Au, W.C., M.J. Crisp, S.Z. DeLuca, O.J. Rando, and M.A. Basrai. 2008. Altered dosage and mislocalization of histone H3 and Cse4p lead to chromosome loss in *Saccharomyces cerevisiae*. *Genetics*. 179:263–275. <https://doi.org/10.1534/genetics.108.088518>
- Au, W.C., A.R. Dawson, D.W. Rawson, S.B. Taylor, R.E. Baker, and M.A. Basrai. 2013. A novel role of the N terminus of budding yeast histone H3 variant Cse4 in ubiquitin-mediated proteolysis. *Genetics*. 194:513–518. <https://doi.org/10.1534/genetics.113.149898>
- Au, W.C., T. Zhang, P.K. Mishra, J.R. Eisenstatt, R.L. Walker, J. Ocampo, A. Dawson, J. Warren, M. Costanzo, A. Baryshnikova, et al. 2020. Skp, Cullin, F-box (SCF)-Met30 and SCF-Cdc4-Mediated Proteolysis of CENP-A Prevents Mislocalization of CENP-A for Chromosomal Stability in Budding Yeast. *PLoS Genet*. 16:e1008597. <https://doi.org/10.1371/journal.pgen.1008597>
- Barnard, D.R., D.K. Kalousek, S.R. Wiersma, B.J. Lange, D.R. Benjamin, D.C. Arthur, J.D. Buckley, N. Kobrinsky, S. Neudorf, J. Sanders, et al. 1996. Morphologic, immunologic, and cytogenetic classification of acute myeloid leukemia and myelodysplastic syndrome in childhood: a report from the Childrens Cancer Group. *Leukemia*. 10:5–12.
- Barnard, D.R., B. Lange, T.A. Alonzo, J. Buckley, J.N. Kobrinsky, S. Gold, S. Neudorf, J. Sanders, L. Burden, and W.G. Woods. 2002. Acute myeloid leukemia and myelodysplastic syndrome in children treated for cancer: comparison with primary presentation. *Blood*. 100:427–434. <https://doi.org/10.1182/blood.V100.2.427>
- Barnhart-Dailey, M.C., P. Trivedi, P.T. Stukenberg, and D.R. Foltz. 2017. HJURP interaction with the condensin II complex during G1 promotes CENP-A deposition. *Mol. Biol. Cell*. 28:54–64. <https://doi.org/10.1091/mbc.e15-12-0843>
- Behrens, J. 1993. The role of cell adhesion molecules in cancer invasion and metastasis. *Breast Cancer Res. Treat.* 24:175–184. <https://doi.org/10.1007/BF01833258>
- Bolger, A.M., M. Lohse, and B. Usadel. 2014. Trimmomatic: a flexible trimmer for Illumina sequence data. *Bioinformatics*. 30:2114–2120. <https://doi.org/10.1093/bioinformatics/btu170>
- Brady, S.T., M. Tytell, and R.J. Lasek. 1984. Axonal tubulin and axonal microtubules: biochemical evidence for cold stability. *J. Cell Biol.* 99:1716–1724. <https://doi.org/10.1083/jcb.99.5.1716>
- Burrell, R.A., S.E. McClelland, D. Endesfelder, P. Groth, M.C. Weller, N. Shaikh, E. Domingo, N. Kanu, S.M. Dewhurst, E. Gronroos, et al. 2013. Replication stress links structural and numerical cancer chromosomal instability. *Nature*. 494:492–496. <https://doi.org/10.1038/nature11935>
- Carroll, C.W., K.J. Milks, and A.F. Straight. 2010. Dual recognition of CENP-A nucleosomes is required for centromere assembly. *J. Cell Biol.* 189:1143–1155. <https://doi.org/10.1083/jcb.201001013>
- Carter, S.L., A.C. Eklund, I.S. Kohane, L.N. Harris, and Z. Szallasi. 2006. A signature of chromosomal instability inferred from gene expression profiles predicts clinical outcome in multiple human cancers. *Nat. Genet.* 38:1043–1048. <https://doi.org/10.1038/ng1861>
- Cheeseman, I.M., J.S. Chappie, E.M. Wilson-Kubalek, and A. Desai. 2006. The conserved KMN network constitutes the core microtubule-binding site of the kinetochore. *Cell*. 127:983–997. <https://doi.org/10.1016/j.cell.2006.09.039>
- Cheng, H., X. Bao, and H. Rao. 2016. The F-box Protein Rcy1 Is Involved in the Degradation of Histone H3 Variant Cse4 and Genome Maintenance. *J. Biol. Chem.* 291:10372–10377. <https://doi.org/10.1074/jbc.M115.701813>
- Choi, E.S., A. Strålfors, S. Catania, A.G. Castillo, J.P. Svensson, A.L. Pidoux, K. Ekwall, and R.C. Allshire. 2012. Factors that promote H3 chromatin integrity during transcription prevent promiscuous deposition of CENP-A(Cnp1) in fission yeast. *PLoS Genet.* 8:e1002985. <https://doi.org/10.1371/journal.pgen.1002985>
- Ciftci-Yilmaz, S., W.C. Au, P.K. Mishra, J.R. Eisenstatt, J. Chang, A.R. Dawson, I. Zhu, M. Rahman, S. Bilke, M. Costanzo, et al. 2018. A Genome-Wide Screen Reveals a Role for the HIR Histone Chaperone Complex in Preventing Mislocalization of Budding Yeast CENP-A. *Genetics*. 210:203–218. <https://doi.org/10.1534/genetics.118.301305>
- Cimini, D., D. Fioravanti, E.D. Salmon, and F. Degross. 2002. Merotelic kinetochore orientation versus chromosome mono-orientation in the origin of lagging chromosomes in human primary cells. *J. Cell Sci.* 115:507–515.
- de Wilde, R.F., C.M. Heaphy, A. Maitra, A.K. Meeker, B.H. Edil, C.L. Wolfgang, T.A. Ellison, R.D. Schulick, I.Q. Molenaar, G.D. Valk, et al. 2012. Loss of ATRX or DAXX expression and concomitant acquisition of the alternative lengthening of telomeres phenotype are late events in a small subset of MEN-1 syndrome pancreatic neuroendocrine tumors. *Mod. Pathol.* 25:1033–1039. <https://doi.org/10.1038/modpathol.2012.53>
- DeLuca, J.G., Y. Dong, P. Hergert, J. Strauss, J.M. Hickey, E.D. Salmon, and B.F. McEwen. 2005. Hec1 and nuf2 are core components of the kinetochore outer plate essential for organizing microtubule attachment sites. *Mol. Biol. Cell*. 16:519–531. <https://doi.org/10.1091/mbc.e04-09-0852>
- Deyter, G.M., and S. Biggins. 2014. The FACT complex interacts with the E3 ubiquitin ligase Psh1 to prevent ectopic localization of CENP-A. *Genes Dev.* 28:1815–1826. <https://doi.org/10.1101/gad.243113.114>
- Dudka, D., A. Noatynska, C.A. Smith, N. Liaudet, A.D. McAnish, and P. Meraldi. 2018. Complete microtubule-kinetochore occupancy favours the segregation of merotelic attachments. *Nat. Commun.* 9:2042. <https://doi.org/10.1038/s41467-018-04427-x>
- Dunleavy, E.M., D. Roche, H. Tagami, N. Lacoste, D. Ray-Gallet, Y. Nakamura, Y. Daigo, Y. Nakatani, and G. Almouzni-Pettinotti. 2009. HJURP is a cell-cycle-dependent maintenance and deposition factor of CENP-A at centromeres. *Cell*. 137:485–497. <https://doi.org/10.1016/j.cell.2009.02.040>
- Eisenstatt, J.R., L. Boeckmann, W.C. Au, V. Garcia, L. Bursch, J. Ocampo, M. Costanzo, M. Weinreich, R.A. Sclafani, A. Baryshnikova, et al. 2020.

- Dbf4-Dependent Kinase (DDK)-Mediated Proteolysis of CENP-A Prevents Mislocalization of CENP-A in *Saccharomyces cerevisiae*. *G3 (Bethesda)*. 10:2057–2068. <https://doi.org/10.1534/g3.120.401131>
- Falk, S.J., L.Y. Guo, N. Sekulic, E.M. Smoak, T. Mani, G.A. Logsdon, K. Gupta, L.E. Jansen, G.D. Van Duyn, S.A. Vinogradov, et al. 2015. CENP-C reshapes and stabilizes CENP-A nucleosomes at the centromere. *Science*. 348:699–703. <https://doi.org/10.1126/science.1259308>
- Foltz, D.R., L.E. Jansen, B.E. Black, A.O. Bailey, J.R. Yates III, and D.W. Cleveland. 2006. The human CENP-A centromeric nucleosome-associated complex. *Nat. Cell Biol.* 8:458–469. <https://doi.org/10.1038/ncb1397>
- Foltz, D.R., L.E. Jansen, A.O. Bailey, J.R. Yates III, E.A. Bassett, S. Wood, B.E. Black, and D.W. Cleveland. 2009. Centromere-specific assembly of CENP-a nucleosomes is mediated by HJURP. *Cell*. 137:472–484. <https://doi.org/10.1016/j.cell.2009.02.039>
- Gascoigne, K.E., K. Takeuchi, A. Suzuki, T. Hori, T. Fukagawa, and I.M. Cheeseman. 2011. Induced ectopic kinetochore assembly bypasses the requirement for CENP-A nucleosomes. *Cell*. 145:410–422. <https://doi.org/10.1016/j.cell.2011.03.031>
- Geigl, J.B., A.C. Obenauf, T. Schwarzbraun, and M.R. Speicher. 2008. Defining ‘chromosomal instability’. *Trends Genet.* 24:64–69. <https://doi.org/10.1016/j.tig.2007.11.006>
- Gkretsi, V., M. Kalli, C. Efstathiades, P. Papageorgis, V. Papanikolaou, L.C. Zacharia, A. Tsezou, E. Athanassiou, and T. Stylianopoulos. 2019. Depletion of Ras Suppressor-1 (RSU-1) promotes cell invasion of breast cancer cells through a compensatory upregulation of a truncated isoform. *Sci. Rep.* 9:10050. <https://doi.org/10.1038/s41598-019-46575-0>
- Gorbsky, G.J., and G.G. Borisy. 1989. Microtubules of the kinetochore fiber turn over in metaphase but not in anaphase. *J. Cell Biol.* 109:653–662. <https://doi.org/10.1083/jcb.109.2.653>
- Gordon, D.J., B. Resio, and D. Pellman. 2012. Causes and consequences of aneuploidy in cancer. *Nat. Rev. Genet.* 13:189–203. <https://doi.org/10.1038/nrg3123>
- Guse, A., C.W. Carroll, B. Moree, C.J. Fuller, and A.F. Straight. 2011. In vitro centromere and kinetochore assembly on defined chromatin templates. *Nature*. 477:354–358. <https://doi.org/10.1038/nature10379>
- Hasson, D., T. Panchenko, K.J. Salimian, M.U. Salman, N. Sekulic, A. Alonso, P.E. Warburton, and B.E. Black. 2013. The octamer is the major form of CENP-A nucleosomes at human centromeres. *Nat. Struct. Mol. Biol.* 20:687–695. <https://doi.org/10.1038/nsmb.2562>
- Hatch, E.M., A.H. Fischer, T.J. Deerinck, and M.W. Hetzer. 2013. Catastrophic nuclear envelope collapse in cancer cell micronuclei. *Cell*. 154:47–60. <https://doi.org/10.1016/j.cell.2013.06.007>
- Henikoff, J.G., J. Thakur, S. Kasinathan, and S. Henikoff. 2015. A unique chromatin complex occupies young α -satellite arrays of human centromeres. *Sci. Adv.* 1:e1400234. <https://doi.org/10.1126/sciadv.1400234>
- Heselmeyer-Haddad, K., L.Y. Berroa Garcia, A. Bradley, C. Ortiz-Melendez, W.J. Lee, R. Christensen, S.A. Prindiville, K.A. Calzone, P.W. Soballe, Y. Hu, et al. 2012. Single-cell genetic analysis of ductal carcinoma in situ and invasive breast cancer reveals enormous tumor heterogeneity yet conserved genomic imbalances and gain of MYC during progression. *Am. J. Pathol.* 181:1807–1822. <https://doi.org/10.1016/j.ajpath.2012.07.012>
- Heun, P., S. Erhardt, M.D. Blower, S. Weiss, A.D. Skora, and G.H. Karpen. 2006. Mislocalization of the Drosophila centromere-specific histone CID promotes formation of functional ectopic kinetochores. *Dev. Cell*. 10:303–315. <https://doi.org/10.1016/j.devcel.2006.01.014>
- Hewawasam, G., M. Shivaraju, M. Mattingly, S. Venkatesh, S. Martin-Brown, L. Florens, J.L. Workman, and J.L. Gerton. 2010. Psh1 is an E3 ubiquitin ligase that targets the centromeric histone variant Cse4. *Mol. Cell*. 40:444–454. <https://doi.org/10.1016/j.molcel.2010.10.014>
- Hoffmann, S., M. Dumont, V. Barra, P. Ly, Y. Nechemia-Arbely, M.A. McMahon, S. Hervé, D.W. Cleveland, and D. Fachinetti. 2016. CENP-A Is Dispensable for Mitotic Centromere Function after Initial Centromere/Kinetochore Assembly. *Cell Rep.* 17:2394–2404. <https://doi.org/10.1016/j.celrep.2016.10.084>
- Hori, T., M. Amano, A. Suzuki, C.B. Backer, J.P. Welburn, Y. Dong, B.F. McEwen, W.H. Shang, E. Suzuki, K. Okawa, et al. 2008. CCAN makes multiple contacts with centromeric DNA to provide distinct pathways to the outer kinetochore. *Cell*. 135:1039–1052. <https://doi.org/10.1016/j.cell.2008.10.019>
- How, C., J. Bruce, J. So, M. Pintilie, B. Haibe-Kains, A. Hui, B.A. Clarke, D.W. Hedley, R.P. Hill, M. Milosevic, et al. 2015. Chromosomal instability as a prognostic marker in cervical cancer. *BMC Cancer*. 15:361. <https://doi.org/10.1186/s12885-015-1372-0>
- Huis in 't Veld, P.J., S. Jeganathan, A. Petrovic, P. Singh, J. John, V. Krenn, F. Weissmann, T. Bange, and A. Musacchio. 2016. Molecular basis of outer kinetochore assembly on CENP-T. *eLife*. 5:e21007.
- Jansen, L.E., B.E. Black, D.R. Foltz, and D.W. Cleveland. 2007. Propagation of centromeric chromatin requires exit from mitosis. *J. Cell Biol.* 176:795–805. <https://doi.org/10.1083/jcb.200701066>
- Kato, H., J. Jiang, B.R. Zhou, M. Rozendaal, H. Feng, R. Ghirlando, T.S. Xiao, A.F. Straight, and Y. Bai. 2013. A conserved mechanism for centromeric nucleosome recognition by centromere protein CENP-C. *Science*. 340:1110–1113. <https://doi.org/10.1126/science.1235532>
- Kinsella, A.R., G.C. Lepts, C.L. Hill, and M. Jones. 1994. Reduced E-cadherin expression correlates with increased invasiveness in colorectal carcinoma cell lines. *Clin. Exp. Metastasis*. 12:335–342. <https://doi.org/10.1007/BF01753841>
- Lacoste, N., A. Woolfe, H. Tachiwana, A.V. Garea, T. Barth, S. Cantaloube, H. Kurumizaka, A. Imhof, and G. Almouzni. 2014. Mislocalization of the centromeric histone variant CenH3/CENP-A in human cells depends on the chaperone DAXX. *Mol. Cell*. 53:631–644. <https://doi.org/10.1016/j.molcel.2014.01.018>
- Lee, A.J., D. Endesfelder, A.J. Rowan, A. Walther, N.J. Birkbak, P.A. Futreal, J. Downward, Z. Szallasi, I.P. Tomlinson, M. Howell, et al. 2011. Chromosomal instability confers intrinsic multidrug resistance. *Cancer Res.* 71:1858–1870. <https://doi.org/10.1158/0008-5472.CAN-10-3604>
- Lengauer, C., K.W. Kinzler, and B. Vogelstein. 1997. Genetic instability in colorectal cancers. *Nature*. 386:623–627. <https://doi.org/10.1038/386623a0>
- Li, Y., Z. Zhu, S. Zhang, D. Yu, H. Yu, L. Liu, X. Cao, L. Wang, H. Gao, and M. Zhu. 2011. ShRNA-targeted centromere protein A inhibits hepatocellular carcinoma growth. *PLoS One*. 6:e17794. <https://doi.org/10.1371/journal.pone.0017794>
- Lim, Z.F., and P.C. Ma. 2019. Emerging insights of tumor heterogeneity and drug resistance mechanisms in lung cancer targeted therapy. *J. Hematol. Oncol.* 12:134. <https://doi.org/10.1186/s13045-019-0818-2>
- Liu, S., M. Kwon, M. Mannino, N. Yang, F. Renda, A. Khodjakov, and D. Pellman. 2018. Nuclear envelope assembly defects link mitotic errors to chromothripsis. *Nature*. 561:551–555. <https://doi.org/10.1038/s41586-018-0534-z>
- Ma, X.J., R. Salunga, J.T. Tuggle, J. Gaudet, E. Enright, P. McQuary, T. Payette, M. Pistone, K. Stecker, B.M. Zhang, et al. 2003. Gene expression profiles of human breast cancer progression. *Proc. Natl. Acad. Sci. USA*. 100:5974–5979. <https://doi.org/10.1073/pnas.0931261100>
- Makrilia, N., A. Kollias, L. Manolopoulos, and K. Syrigos. 2009. Cell adhesion molecules: role and clinical significance in cancer. *Cancer Invest.* 27:1023–1037. <https://doi.org/10.3109/07357900902769749>
- Marshall, O.J., A.C. Chueh, L.H. Wong, and K.A. Choo. 2008. Neocentromeres: new insights into centromere structure, disease development, and karyotype evolution. *Am J Hum Genet.* 82:261–282. <https://doi.org/10.1016/j.ajhg.2007.11.009>
- Maurici, D., A. Perez-Atayde, H.E. Grier, N. Baldini, M. Serra, and J.A. Fletcher. 1998. Frequency and implications of chromosome 8 and 12 gains in Ewing sarcoma. *Cancer Genet. Cytogenet.* 100:106–110. [https://doi.org/10.1016/S0165-4608\(97\)00028-9](https://doi.org/10.1016/S0165-4608(97)00028-9)
- McGovern, S.L., Y. Qi, L. Pusztai, W.F. Symmans, and T.A. Buchholz. 2012. Centromere protein-A, an essential centromere protein, is a prognostic marker for relapse in estrogen receptor-positive breast cancer. *Breast Cancer Res.* 14:R72. <https://doi.org/10.1186/bcr3181>
- Mendiburo, M.J., J. Padeken, S. Fülöp, A. Schepers, and P. Heun. 2011. Drosophila CenH3 is sufficient for centromere formation. *Science*. 334:686–690. <https://doi.org/10.1126/science.1206880>
- Mierke, C.T., P. Kollmannsberger, D.P. Zitterbart, G. Diez, T.M. Koch, S. Marg, W.H. Ziegler, W.H. Goldmann, and B. Fabry. 2010. Vinculin facilitates cell invasion into three-dimensional collagen matrices. *J. Biol. Chem.* 285:13121–13130. <https://doi.org/10.1074/jbc.M109.087171>
- Mitchison, T.J., and E.D. Salmon. 1992. Poleward kinetochore fiber movement occurs during both metaphase and anaphase-A in newt lung cell mitosis. *J. Cell Biol.* 119:569–582. <https://doi.org/10.1083/jcb.119.3.569>
- Moh, M.C., and S. Shen. 2009. The roles of cell adhesion molecules in tumor suppression and cell migration: a new paradox. *Cell Adhes. Migr.* 3:334–336. <https://doi.org/10.4161/cam.3.4.9246>
- Moree, B., C.B. Meyer, C.J. Fuller, and A.F. Straight. 2011. CENP-C recruits M18BP1 to centromeres to promote CENP-A chromatin assembly. *J. Cell Biol.* 194:855–871. <https://doi.org/10.1083/jcb.201106079>
- Müller, S., R. Montes de Oca, N. Lacoste, F. Dingli, D. Loew, and G. Almouzni. 2014. Phosphorylation and DNA binding of HJURP determine its

- centromeric recruitment and function in CenH3(CENP-A) loading. *Cell Rep.* 8:190–203. <https://doi.org/10.1016/j.celrep.2014.06.002>
- Nardi, I.K., E. Zasadzińska, M.E. Stellfox, C.M. Knippler, and D.R. Foltz. 2016. Licensing of Centromeric Chromatin Assembly through the Misl8a-Misl8β Heterotetramer. *Mol. Cell.* 61:774–787. <https://doi.org/10.1016/j.molcel.2016.02.014>
- Nechemia-Arbely, Y., K.H. Miga, O. Shoshani, A. Aslanian, M.A. McMahon, A.Y. Lee, D. Fachinetti, J.R. Yates III, B. Ren, and D.W. Cleveland. 2019. DNA replication acts as an error correction mechanism to maintain centromere identity by restricting CENP-A to centromeres. *Nat. Cell Biol.* 21:743–754. <https://doi.org/10.1038/s41556-019-0331-4>
- Nishino, T., F. Rago, T. Hori, K. Tomii, I.M. Cheeseman, and T. Fukagawa. 2013. CENP-T provides a structural platform for outer kinetochore assembly. *EMBO J.* 32(3):424–436. <https://doi.org/10.1038/emboj.2012.348>
- Nishino, T., K. Takeuchi, K.E. Gascoigne, A. Suzuki, T. Hori, T. Oyama, K. Morikawa, I.M. Cheeseman, and T. Fukagawa. 2012. CENP-T-W-S-X forms a unique centromeric chromatin structure with a histone-like fold. *Cell.* 148:487–501. <https://doi.org/10.1016/j.cell.2011.11.061>
- Nye, J., D. Sturgill, R. Athwal, and Y. Dalal. 2018. HJURP antagonizes CENP-A mislocalization driven by the H3.3 chaperones HIRA and DAXX. *PLoS One.* 13:e0205948. <https://doi.org/10.1371/journal.pone.0205948>
- Ohkuni, K., R. Abdulle, and K. Kitagawa. 2014. Degradation of centromeric histone H3 variant Cse4 requires the Fpr3 peptidyl-prolyl Cis-Trans isomerase. *Genetics.* 196:1041–1045. <https://doi.org/10.1534/genetics.114.161224>
- Ohkuni, K., Y. Takahashi, A. Fulp, J. Lawrimore, W.C. Au, N. Pasupala, R. Levy-Myers, J. Warren, A. Strunnikov, R.E. Baker, et al. 2016. SUMO-Targeted Ubiquitin Ligase (STUbL) Slx5 regulates proteolysis of centromeric histone H3 variant Cse4 and prevents its mislocalization to euchromatin. *Mol. Biol. Cell.* 27:1500–1510. <https://doi.org/10.1091/mbc.E15-12-0827>
- Ohkuni, K., E. Suva, W.C. Au, R.L. Walker, R. Levy-Myers, P.S. Meltzer, R.E. Baker, and M.A. Basrai. 2020. Deposition of Centromeric Histone H3 Variant CENP-A/Cse4 into Chromatin Is Facilitated by Its C-Terminal Sumoylation. *Genetics.* 214:839–854. <https://doi.org/10.1534/genetics.120.303090>
- Okada, M., I.M. Cheeseman, T. Hori, K. Okawa, I.X. McLeod, J.R. Yates III, A. Desai, and T. Fukagawa. 2006. The CENP-H-I complex is required for the efficient incorporation of newly synthesized CENP-A into centromeres. *Nat. Cell Biol.* 8:446–457. <https://doi.org/10.1038/ncb1396>
- Oltmann, J., K. Hesselmeier-Haddad, L.S. Hernandez, R. Meyer, I. Torres, Y. Hu, N. Doberstein, J.K. Killian, D. Petersen, Y.J. Zhu, et al. 2018. Aneuploidy, TP53 mutation, and amplification of MYC correlate with increased intratumor heterogeneity and poor prognosis of breast cancer patients. *Genes Chromosomes Cancer.* 57:165–175. <https://doi.org/10.1002/gcc.22515>
- Pan, W.W., F.P. Yi, L.X. Cao, X.M. Liu, Z.F. Shen, Y.Q. Bu, Y. Xu, H.Y. Fan, and F.Z. Song. 2013a. DAXX silencing suppresses mouse ovarian surface epithelial cell growth by inducing senescence and DNA damage. *Gene.* 526:287–294. <https://doi.org/10.1016/j.gene.2013.03.103>
- Pan, W.W., J.J. Zhou, X.M. Liu, Y. Xu, L.J. Guo, C. Yu, Q.H. Shi, and H.Y. Fan. 2013b. Death domain-associated protein DAXX promotes ovarian cancer development and chemoresistance. *J. Biol. Chem.* 288:13620–13630. <https://doi.org/10.1074/jbc.M112.446369>
- Pan, D., K. Walstein, A. Take, D. Bier, N. Kaiser, and A. Musacchio. 2019. Mechanism of centromere recruitment of the CENP-A chaperone HJURP and its implications for centromere licensing. *Nat. Commun.* 10: 4046. <https://doi.org/10.1038/s41467-019-12019-6>
- Paulsson, K., and B. Johansson. 2007. Trisomy 8 as the sole chromosomal aberration in acute myeloid leukemia and myelodysplastic syndromes. *Pathol. Biol. (Paris).* 55:37–48. <https://doi.org/10.1016/j.patbio.2006.04.007>
- Perpelescu, M., and T. Fukagawa. 2011. The ABCs of CENPs. *Chromosoma.* 120: 425–446. <https://doi.org/10.1007/s00412-011-0330-0>
- Pfister, K., J.L. Pipka, C. Chiang, Y. Liu, R.A. Clark, R. Keller, P. Skoglund, M.J. Guertin, I.M. Hall, and P.T. Stukenberg. 2018. Identification of Drivers of Aneuploidy in Breast Tumors. *Cell Rep.* 23:2758–2769. <https://doi.org/10.1016/j.celrep.2018.04.102>
- Przewłoka, M.R., Z. Venkei, V.M. Bolanos-Garcia, J. Debski, M. Dadlez, and D.M. Glover. 2011. CENP-C is a structural platform for kinetochore assembly. *Curr. Biol.* 21:399–405. <https://doi.org/10.1016/j.cub.2011.02.005>
- Puto, L.A., J. Brognard, and T. Hunter. 2015. Transcriptional Repressor DAXX Promotes Prostate Cancer Tumorigenicity via Suppression of Autophagy. *J. Biol. Chem.* 290:15406–15420. <https://doi.org/10.1074/jbc.M115.658765>
- Qi, H., P. Dal Cin, J.M. Hernández, J.L. García, R. Sciort, C. Fletcher, P. Van Eyken, I. De Wever, and H. Van den Berghe. 1996. Trisomies 8 and 20 in desmoid tumors. *Cancer Genet. Cytogenet.* 92:147–149. [https://doi.org/10.1016/S0165-4608\(96\)00170-7](https://doi.org/10.1016/S0165-4608(96)00170-7)
- Rajput, A.B., N. Hu, S. Varma, C.H. Chen, K. Ding, P.C. Park, J.A. Chapman, S.K. Sengupta, Y. Madarnas, B.E. Elliott, and H.E. Feilottter. 2011. Immunohistochemical Assessment of Expression of Centromere Protein-A (CENPA) in Human Invasive Breast Cancer. *Cancers (Basel).* 3: 4212–4227. <https://doi.org/10.3390/cancers304212>
- Ranjitkar, P., M.O. Press, X. Yi, R. Baker, M.J. MacCoss, and S. Biggins. 2010. An E3 ubiquitin ligase prevents ectopic localization of the centromeric histone H3 variant via the centromere targeting domain. *Mol. Cell.* 40: 455–464. <https://doi.org/10.1016/j.molcel.2010.09.025>
- Saha, A.K., R. Contreras-Galindo, Y.S. Niknafs, M. Iyer, T. Qin, K. Padmanabhan, J. Siddiqui, M. Palande, C. Wang, B. Qian, et al. 2020. The role of the histone H3 variant CENPA in prostate cancer. *J. Biol. Chem.* 295: 8537–8549. <https://doi.org/10.1074/jbc.RA119.010080>
- Sathyan, K.M., D. Fachinetti, and D.R. Foltz. 2017. α-amino trimethylation of CENP-A by NRM1 is required for full recruitment of the centromere. *Nat. Commun.* 8:14678. <https://doi.org/10.1038/ncomms14678>
- Schmidt, J.C., T. Kiyomitsu, T. Hori, C.B. Backer, T. Fukagawa, and I.M. Cheeseman. 2010. Aurora B kinase controls the targeting of the Astrin-SKAP complex to bioriented kinetochores. *J. Cell Biol.* 191:269–280. <https://doi.org/10.1083/jcb.201006129>
- Screpanti, E., A. De Antoni, G.M. Alushin, A. Petrovic, T. Melis, E. Nogales, and A. Musacchio. 2011. Direct binding of Cenp-C to the Misl2 complex joins the inner and outer kinetochore. *Curr. Biol.* 21:391–398. <https://doi.org/10.1016/j.cub.2010.12.039>
- Shrestha, R.L., and V.M. Draviam. 2013. Lateral to end-on conversion of chromosome-microtubule attachment requires kinesins CENP-E and MCAK. *Curr. Biol.* 23:1514–1526. <https://doi.org/10.1016/j.cub.2013.06.040>
- Shrestha, R.L., G.S. Ahn, M.I. Staples, K.M. Sathyan, T.S. Karpova, D.R. Foltz, and M.A. Basrai. 2017a. Mislocalization of centromeric histone H3 variant CENP-A contributes to chromosomal instability (CIN) in human cells. *Oncotarget.* 8:46781–46800. <https://doi.org/10.18632/oncotarget.18108>
- Shrestha, R.L., D. Conti, N. Tamura, D. Braun, R.A. Ramalingam, K. Cieslinski, J. Ries, and V.M. Draviam. 2017b. Aurora-B kinase pathway controls the lateral to end-on conversion of kinetochore-microtubule attachments in human cells. *Nat. Commun.* 8:150. <https://doi.org/10.1038/s41467-017-00209-z>
- Siegel, J.J., and A. Amon. 2012. New insights into the troubles of aneuploidy. *Annu. Rev. Cell Dev. Biol.* 28:189–214. <https://doi.org/10.1146/annurev-cellbio-101011-155807>
- Stangeland, B., A.A. Mughal, Z. Grieg, C.J. Sandberg, M. Joel, S. Nygård, T. Meling, W. Murrell, E.O. Vik Mo, and I.A. Langmoen. 2015. Combined expression analysis, bioinformatics and targeted proteomics identify new potential therapeutic targets in glioblastoma stem cells. *Oncotarget.* 6:26192–26215. <https://doi.org/10.18632/oncotarget.4613>
- Subramanian, A., P. Tamayo, V.K. Mootha, S. Mukherjee, B.L. Ebert, M.A. Gillette, A. Paulovich, S.L. Pomeroy, T.R. Golub, E.S. Lander, and J.P. Mesirov. 2005. Gene set enrichment analysis: a knowledge-based approach for interpreting genome-wide expression profiles. *Proc. Natl. Acad. Sci. USA.* 102:15545–15550. <https://doi.org/10.1073/pnas.0506580102>
- Sulzer, M.A., M.P. Leers, J.A. van Noord, E.C. Bollen, and P.H. Theunissen. 1998. Reduced E-cadherin expression is associated with increased lymph node metastasis and unfavorable prognosis in non-small cell lung cancer. *Am. J. Respir. Crit. Care Med.* 157:1319–1323. <https://doi.org/10.1164/ajrccm.157.4.9703099>
- Sun, X., P.L. Clermont, W. Jiao, C.D. Helgason, P.W. Gout, Y. Wang, and S. Qu. 2016. Elevated expression of the centromere protein-A(CENP-A)-encoding gene as a prognostic and predictive biomarker in human cancers. *Int. J. Cancer.* 139:899–907. <https://doi.org/10.1002/ijc.30133>
- Sundin, L.J., G.J. Guimaraes, and J.G. Deluca. 2011. The NDC80 complex proteins Nuf2 and Hec1 make distinct contributions to kinetochore-microtubule attachment in mitosis. *Mol. Biol. Cell.* 22:759–768. <https://doi.org/10.1091/mbc.e10-08-0671>
- Suzuki, A., B.L. Badger, and E.D. Salmon. 2015. A quantitative description of Ndc80 complex linkage to human kinetochores. *Nat. Commun.* 6:8161. <https://doi.org/10.1038/ncomms9161>

- Thompson, S.L., S.F. Bakhoum, and D.A. Compton. 2010. Mechanisms of chromosomal instability. *Curr. Biol.* 20:R285–R295. <https://doi.org/10.1016/j.cub.2010.01.034>
- Tomonaga, T., K. Matsushita, S. Yamaguchi, T. Oohashi, H. Shimada, T. Ochiai, K. Yoda, and F. Nomura. 2003. Overexpression and mistargeting of centromere protein-A in human primary colorectal cancer. *Cancer Res.* 63:3511–3516.
- Trapnell, C., L. Pachter, and S.L. Salzberg. 2009. TopHat: discovering splice junctions with RNA-Seq. *Bioinformatics.* 25:1105–1111. <https://doi.org/10.1093/bioinformatics/btp120>
- Turajlic, S., and C. Swanton. 2016. Metastasis as an evolutionary process. *Science.* 352:169–175. <https://doi.org/10.1126/science.aaf2784>
- Uchida, K.S., K. Takagaki, K. Kumada, Y. Hirayama, T. Noda, and T. Hirota. 2009. Kinetochore stretching inactivates the spindle assembly checkpoint. *J. Cell Biol.* 184:383–390. <https://doi.org/10.1083/jcb.200811028>
- Van Hooser, A.A., I.I. Ouspenski, H.C. Gregson, D.A. Starr, T.J. Yen, M.L. Goldberg, K. Yokomori, W.C. Earnshaw, K.F. Sullivan, and B.R. Brinkley. 2001. Specification of kinetochore-forming chromatin by the histone H3 variant CENP-A. *J. Cell Sci.* 114:3529–3542.
- Vleminckx, K., L. Vakaet Jr., M. Mareel, W. Fiers, and F. van Roy. 1991. Genetic manipulation of E-cadherin expression by epithelial tumor cells reveals an invasion suppressor role. *Cell.* 66:107–119. [https://doi.org/10.1016/0092-8674\(91\)90143-M](https://doi.org/10.1016/0092-8674(91)90143-M)
- Wang, Y., J.G. Klijn, Y. Zhang, A.M. Sieuwerts, M.P. Look, F. Yang, D. Tantalov, M. Timmermans, M.E. Meijer-van Gelder, J. Yu, et al. 2005. Gene-expression profiles to predict distant metastasis of lymph-node-negative primary breast cancer. *Lancet.* 365:671–679. [https://doi.org/10.1016/S0140-6736\(05\)17947-1](https://doi.org/10.1016/S0140-6736(05)17947-1)
- Xu, J., L. Huang, and J. Li. 2016. DNA aneuploidy and breast cancer: a meta-analysis of 141,163 cases. *Oncotarget.* 7:60218–60229. <https://doi.org/10.18632/oncotarget.11130>
- Ye, C.J., Z. Sharpe, S. Alemara, S. Mackenzie, G. Liu, B. Abdallah, S. Horne, S. Regan, and H.H. Heng. 2019. Micronuclei and Genome Chaos: Changing the System Inheritance. *Genes (Basel).* 10:366. <https://doi.org/10.3390/genes10050366>
- Zasadzińska, E., J. Huang, A.O. Bailey, L.Y. Guo, N.S. Lee, S. Srivastava, K.A. Wong, B.T. French, B.E. Black, and D.R. Foltz. 2018. Inheritance of CENP-A Nucleosomes during DNA Replication Requires HJURP. *Dev. Cell.* 47:348–362.e7. <https://doi.org/10.1016/j.devcel.2018.09.003>
- Zhang, C.Z., A. Spektor, H. Cornils, J.M. Francis, E.K. Jackson, S. Liu, M. Meyerson, and D. Pellman. 2015. Chromothripsis from DNA damage in micronuclei. *Nature.* 522:179–184. <https://doi.org/10.1038/nature14493>
- Zhang, W., J.H. Mao, W. Zhu, A.K. Jain, K. Liu, J.B. Brown, and G.H. Karpen. 2016. Centromere and kinetochore gene misexpression predicts cancer patient survival and response to radiotherapy and chemotherapy. *Nat. Commun.* 7:12619. <https://doi.org/10.1038/ncomms12619>
- Zhou, Z., H.S. Zhang, Y. Liu, Z.G. Zhang, G.Y. Du, H. Li, X.Y. Yu, and Y.H. Huang. 2018. Loss of TET1 facilitates DLD1 colon cancer cell migration via H3K27me3-mediated down-regulation of E-cadherin. *J. Cell. Physiol.* 233:1359–1369. <https://doi.org/10.1002/jcp.26012>
- Zhu, J., H.J. Tsai, M.R. Gordon, and R. Li. 2018. Cellular Stress Associated with Aneuploidy. *Dev. Cell.* 44:420–431. <https://doi.org/10.1016/j.devcel.2018.02.002>

Supplemental material

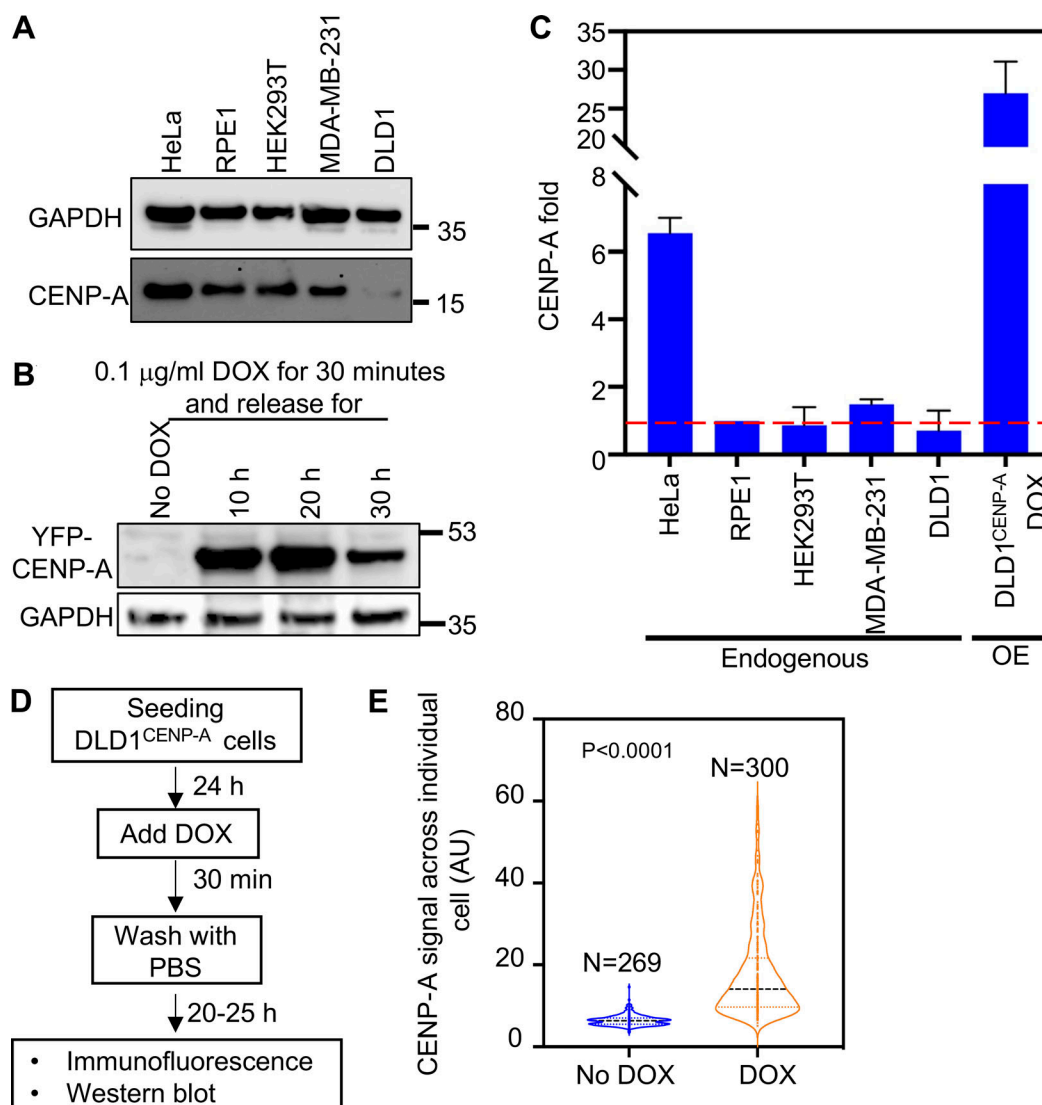


Figure S1. **Optimization of DOX treatment and CENP-A expression.** (A) Levels of endogenous CENP-A in different cell lines. Western blot shows levels of endogenous CENP-A in different cell lines as indicated. Blot was probed with anti-CENP-A antibody. GAPDH was used as a loading control. Three biological repeats were performed. (B) Expression of CENP-A in DOX-treated DLD1^{CENP-A} cells. Western blot shows levels of YFP-CENP-A in DLD1^{CENP-A} cells treated with 0.1 µg/ml DOX and after various time points post-DOX wash. Blot was probed with anti-GFP antibody. GAPDH was used as a loading control. (C) Quantification of endogenous and exogenous CENP-A levels. Bar chart shows the levels of endogenous CENP-A in different cell lines as in A and the levels of exogenously OE CENP-A in DLD1^{CENP-A} cells treated with DOX for 30 min followed by DOX removal for 20 h as in B. The levels of CENP-A normalized against the loading control, GAPDH, were compared as fold increase. Error bar represents SEM from two independent experiments. (D) Flowchart showing the experimental regimen for treatment with DOX used for all studies unless otherwise described. (E) CENP-A signal intensity is higher in DOX-treated DLD1^{CENP-A} cells. Violin plot showing the spectrum of CENP-A signal intensity across individual DLD1^{CENP-A} cells with or without DOX treatment. P values calculated by using the unpaired Student's *t* test are indicated.

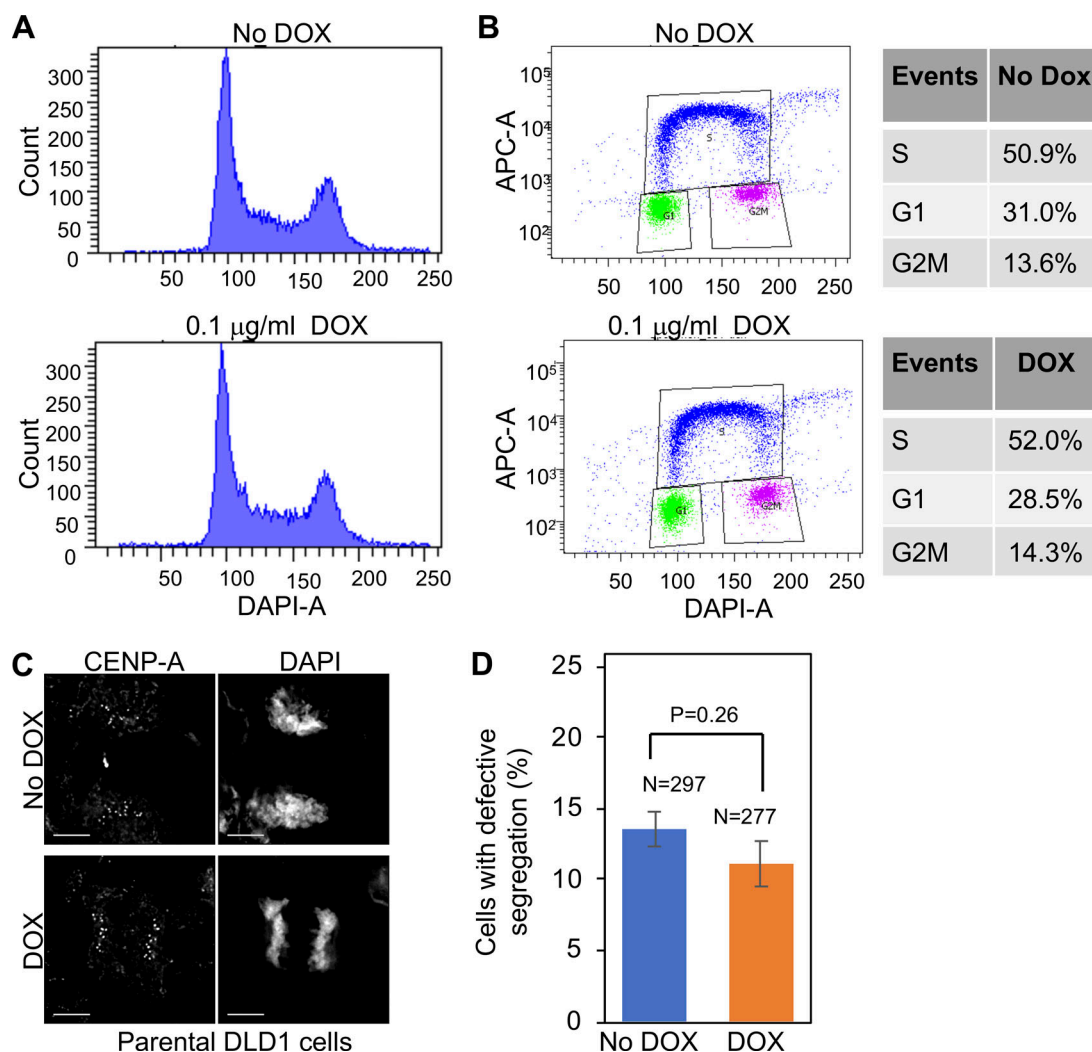


Figure S2. DOX-induced overexpression of CENP-A does not contribute to cell-cycle defects in DLD1^{CENP-A} cells. (A) CENP-A OE does not lead to defects in cell-cycle progression. Flow cytometry analysis of DLD1^{CENP-A} cells with or without DOX treatment shows similar cell-cycle profiles with 2N (G1/S stage) and 4N (G2/M stage) DNA content. **(B)** CENP-A OE does not contribute to reduced cell proliferation. Flow cytometry plot showing the distribution of EdU-stained DLD1^{CENP-A} cells with or without DOX treatment in different cell-cycle stages. Results were confirmed by using three biological repeats. Tables show the absolute percentage of cells in different cell-cycle stages. **(C)** DOX treatment does not increase chromosome segregation defects in parental DLD1 cells. Images show chromosome segregation status in parental DLD1 cells with or without DOX treatment. Cells were immunostained with antibodies against CENP-A and stained with DAPI. Cells were then analyzed for chromosome segregation outcome. Scale bar: 5 μ m. **(D)** Quantification shows the proportion of cells with defective segregation in parental DLD1 cells treated as in F. Error bars represent SEM from three independent experiments. "N" denotes number of cells analyzed. P values calculated by using the unpaired Student's *t* test are indicated.

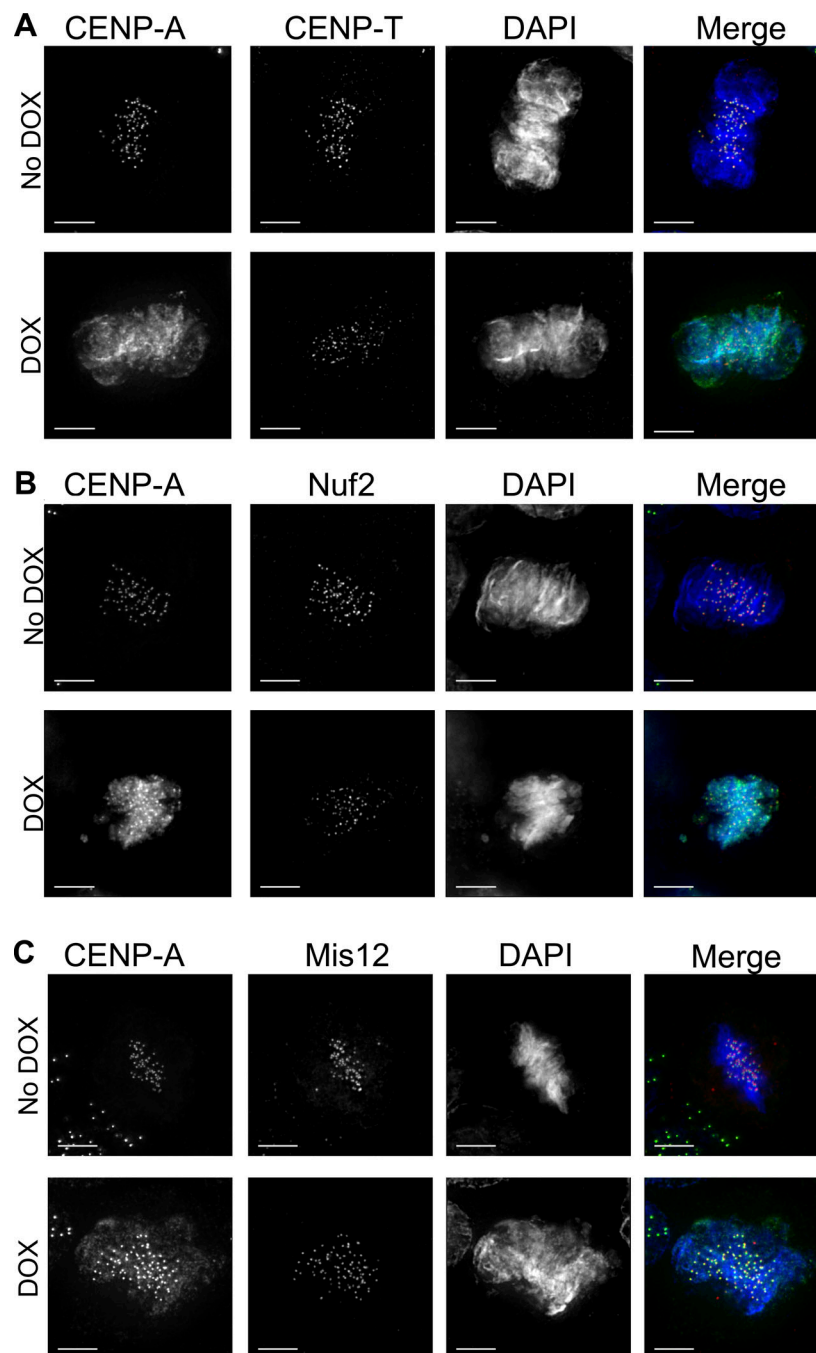


Figure S3. CENP-A OE contributes to reduced kinetochore localization of CENP-T, NUF2, and Mis12 in DLD1^{CENP-A} cells. (A) Reduced centromeric CENP-T signal intensities in DLD1^{CENP-A} cells with overexpressed and mislocalized CENP-A. Images of CENP-T localization at centromeres on metaphase plates in DLD1^{CENP-A} cells with or without DOX treatment. (B) Reduced kinetochore NUF2 signal intensities in DLD1^{CENP-A} cells with overexpressed and mislocalized CENP-A. Images of NUF2 localization at kinetochores on metaphase plates in DLD1^{CENP-A} cells with or without DOX treatment. (C) Reduced centromeric localization of Mis12 in DLD1^{CENP-A} cells with overexpressed and mislocalized CENP-A. Images of localization of Mis12 at kinetochores on metaphase plates in DLD1^{CENP-A} cells with or without DOX treatment. For all panels in this figure, before immunostaining, cells were treated with 10 μM MG132 for 90 min, followed by fixation with ice-cold methanol for 1 min and immunostaining with antibodies as indicated. Cells were stained with DAPI. Scale bar: 5 μm.

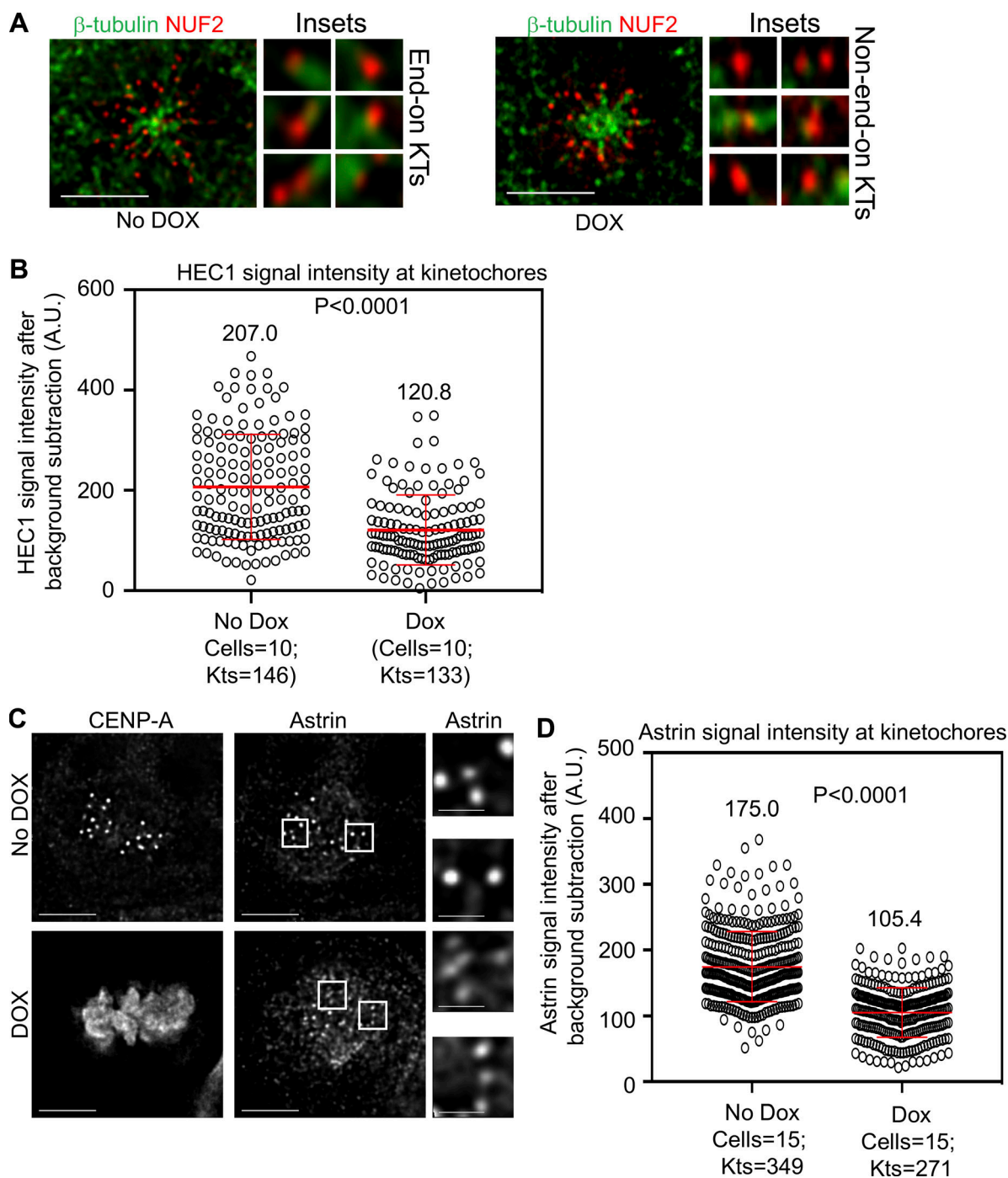


Figure S4. CENP-A OE contributes to reduced levels of HEC1 and Astrin at kinetochores. (A) Reduced levels of stable end-on attached kinetochores in DLD1^{CENP-A} cells with overexpressed CENP-A. Images show KT-MT attachment status in DLD1^{CENP-A} cells with or without DOX treatment. Prior to fixation with ice-cold methanol for 1 min, cells were treated with 10 μ M monastrol (3 h) and 10 μ M MG132 (90 min), followed by exposure to cold for 10 min. Cells were immunostained with antibodies against NUF2 and β -tubulin and analyzed for kinetochores with end-on (stable and cold resistant) or non-end-on attachment (unstable and cold sensitive) to microtubules. Insets correspond to white-boxed areas in main images. Scale bar: 5 μ m (main figures). (B) Reduced levels of HEC1 in DLD1 cells with overexpressed CENP-A. Prism graph for quantification of HEC1 signal intensity at kinetochores in DLD1^{CENP-A} cells with or without DOX treatment as in Fig. 4 E. (C) Reduced Astrin signal intensity at congressed kinetochores on metaphase plate in DLD1 cells with overexpressed CENP-A. Images show signal intensity of Astrin at kinetochores in DLD1^{CENP-A} cells with or without DOX treatment. Prior to immunostaining, cells were treated with 10 μ M MG132 for 90 min. Cells were immunostained with antibodies against CENP-A and Astrin, and Astrin signal intensity was quantified at congressed kinetochores on metaphase plates. Insets correspond to white-boxed areas in main images. Scale bar: 5 μ m (main images), 2 μ m (insets). (D) Prism graph shows Astrin signal intensity at kinetochores in DLD1^{CENP-A} cells with or without DOX treatment. In all prism graphs, each circle represents each kinetochore. "Kts" denotes the number of kinetochore pairs analyzed in number of cells as denoted by "Cells." Red horizontal lines represent mean signal intensities. Error bars represent SD measured across kinetochores in the indicated number of cells from at least two independent experiments. P values calculated by using the Mann-Whitney U test are indicated.

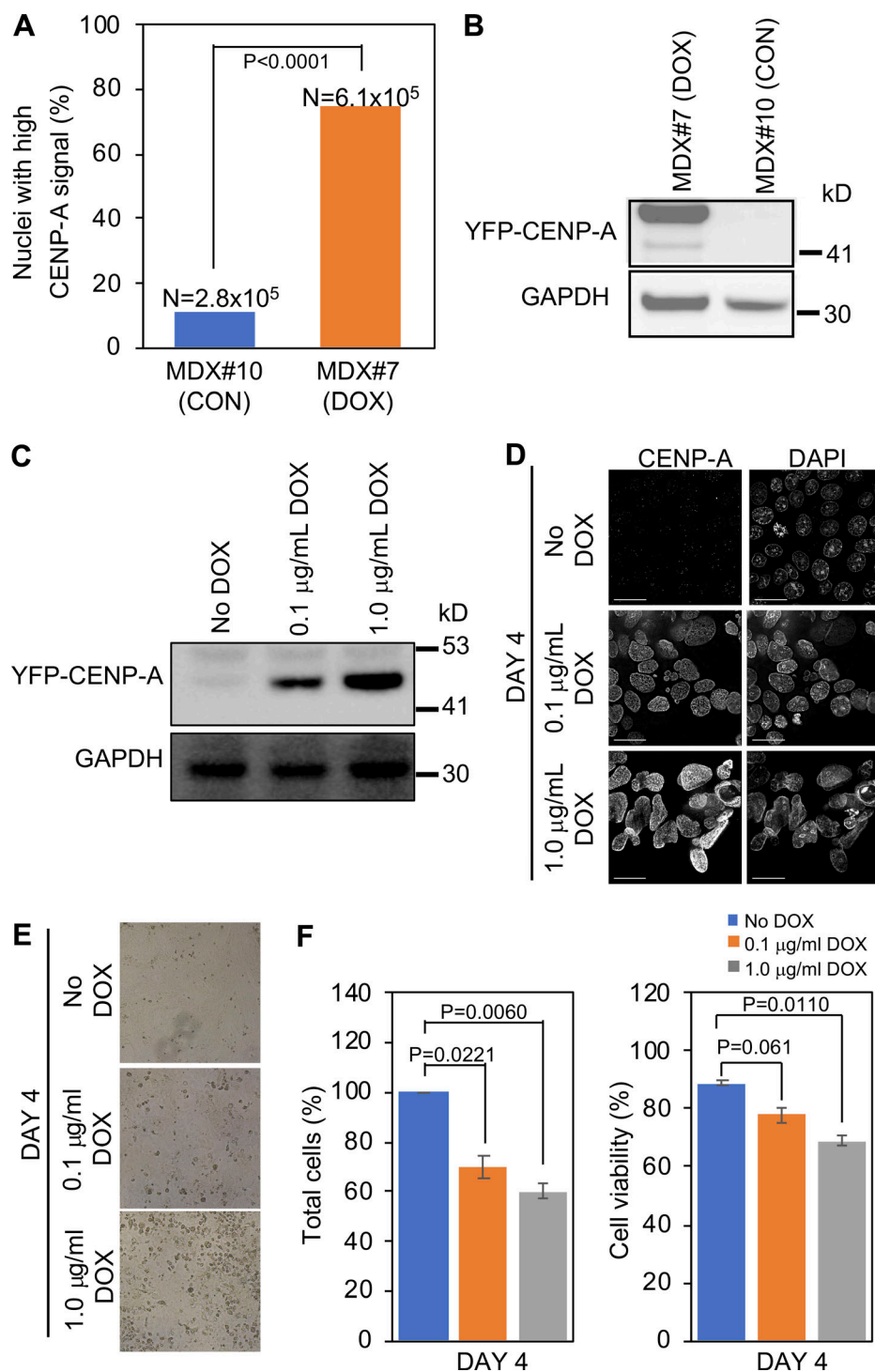


Figure S5. **High levels of CENP-A in xenograft tumor tissues and in cultured DLD1 cells.** (A) CENP-A-positive nuclei are higher in xenograft tissue derived from mouse fed with the DOX diet. Bar chart shows proportion of CENP-A-positive nuclei analyzed from IHC images as in Fig. 7B. "N" denotes numbers of cells analyzed. P value was calculated by using the χ^2 test. (B) Levels of YFP-CENP-A in tumor tissue of mouse on DOX diet. Western blots show levels of YFP-CENP-A in nuclear extracts collected from tumor tissues of MDX#07 or MDX#10 mice. (C) Dose-dependent OE of YFP-CENP-A in DLD1 cells. Western blots show protein levels of YFP-CENP-A in DLD1^{CENP-A} cells with or without 0.1 µg/ml or 1.0 µg/ml DOX treatment for 4 d. Blots were probed with anti-GFP antibody for expression of YFP-CENP-A, and anti-GAPDH antibody was used for loading control. (D) Higher mislocalization of YFP-CENP-A in DLD1 cells treated with 1.0 µg/ml DOX for 4 d. Images show YFP-CENP-A localization in DLD1^{CENP-A} cells treated as in A. Cells were immunostained with antibodies against CENP-A and stained with DAPI. (E) Reduced cell viability in cells with constitutive high OE of CENP-A. Brightfield microscopic images show viability status of DLD1^{CENP-A} cells treated as in C. (F) Total cell population and cell viability are reduced in DLD1^{CENP-A} cells treated with 1.0 µg/ml DOX. Bar charts show the proportion of total cells (left) and viable cells (right) in DLD1^{CENP-A} cells treated with indicated concentrations of DOX for 4 d. Error bars represent SEM from three independent experiments. P values calculated by using unpaired Student's *t* test are indicated.

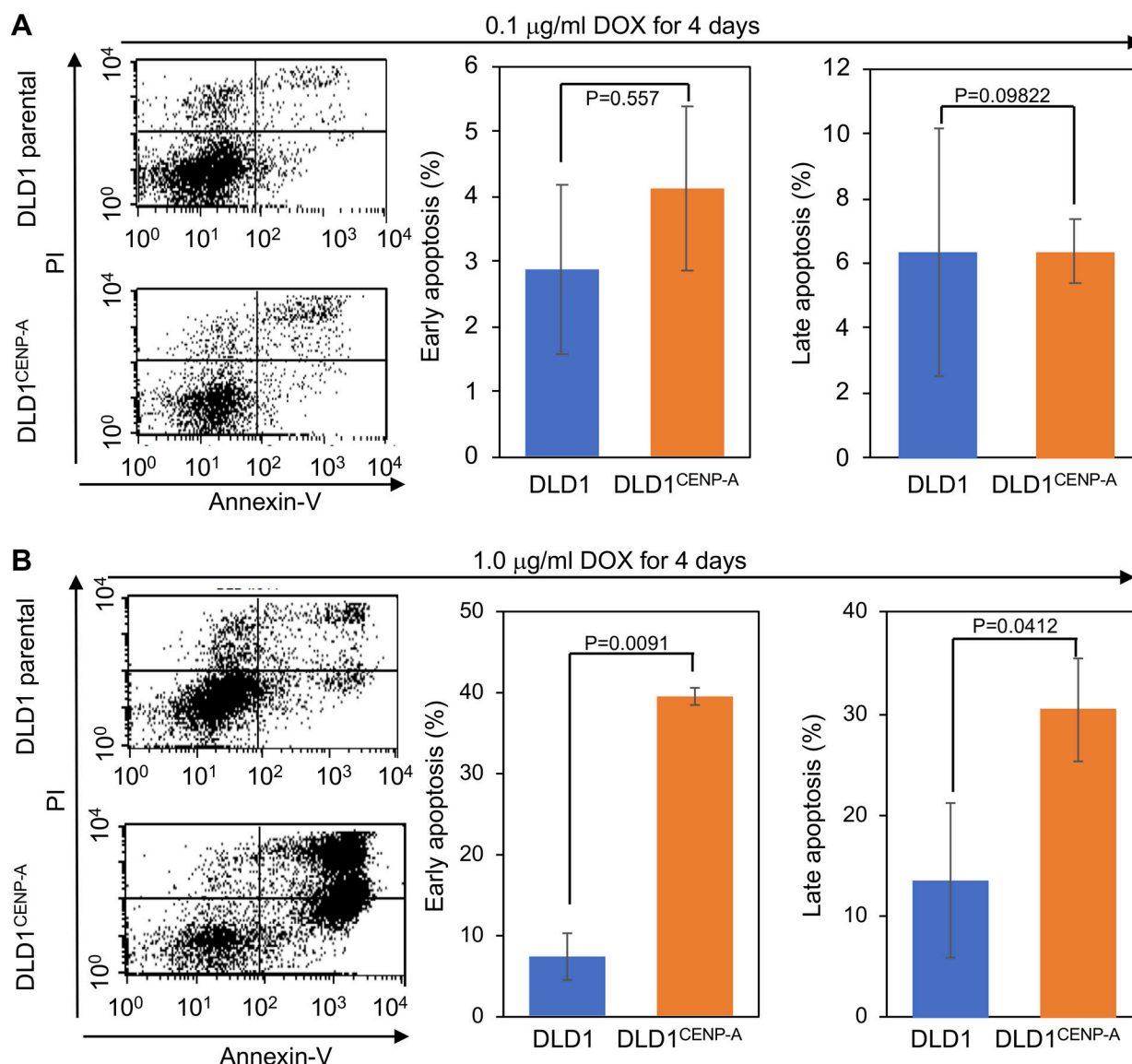


Figure S6. Constitutive high levels of CENP-A OE contribute to apoptosis in DLD1 cells. (A) Constitutive low levels of CENP-A OE do not induce apoptosis in DLD1^{CENP-A} cells. Flow cytometry analysis and quantification show the proportion of cells that are positive for Annexin and/or PI in DLD1^{CENP-A} or parental DLD1 cells with or without 0.1 µg/ml DOX treatment for 4 d. DOX was replenished every 2 d for constitutive overexpression of YFP-CENP-A. **(B)** Constitutive high levels of CENP-A OE induces apoptosis in DLD1^{CENP-A} cells. Flow cytometry analysis and quantification show a high proportion of cells that are positive for Annexin and/or PI in DLD1^{CENP-A} cells with 1.0 µg/ml DOX for 4 d compared with parental DLD1 cells without DOX treatment. Live cells were stained with Annexin V or PI and analyzed in flow cytometry. Error bars represent SEM from three independent experiments. P values were calculated by using unpaired Student's *t* test.

Video 1. Time lapse images of DOX-treated DLD1^{CENP-A} cells in prometaphase entering into metaphase and exiting from mitosis with lagging chromosomes. DLD1^{CENP-A} cells were grown on a glass-bottom imaging dish in RPMI media for 48 h. Cells were then treated with DOX for 30 min, followed by DOX wash off, and were grown further for 20 h. Before imaging, RPMI media was removed and replaced with Leobovitz (L-15) medium without antibiotics. Cells were then imaged with FITC (Ex 490/20; Em 528/38) to visualize YFP-CENP-A and DIC with exposure of 50% for 0.2 s. Cells were imaged at the time interval of 10 min for 5 h.

Video 2. **Time-lapse images of DOX-treated DLD1^{CENP-A} cells in prometaphase entering into metaphase and exiting from mitosis, eventually forming the micronuclei.** DLD1^{CENP-A} cells were grown on a glass-bottom imaging dish in RPMI media for 48 h. Cells were then treated with DOX for 30 min, followed by DOX wash off, and were grown further for 20 h. Before imaging, RPMI media was removed and replaced with Leobovitz (L-15) medium without antibiotics. Cells were then imaged with FITC (Ex 490/20; Em 528/38) to visualize YFP-CENP-A and DIC with exposure of 50% for 0.2 s. Cells were imaged at the time interval of 10 min for 5 h.

Video 3. **3D-reconstructed image of DLD1^{CENP-A} cells without DOX treatment as in Fig. 4 E showing Astrin-positive kinetochores.** DLD1^{CENP-A} cells were grown in RPMI media on glass coverslips in a 12-well tissue culture dish for 72 h. Cells were fixed with ice-cold methanol for 1 min. Cells immunostained with antibodies against Astrin and HEC1. 3D rendering was performed with Imaris 9.5.0.

Video 4. **3D-reconstructed images of DLD1^{CENP-A} cells with DOX treatment as in Fig. 4 E showing kinetochores devoid of Astrin.** DLD1^{CENP-A} cells were grown in RPMI media on glass coverslips in a 12-well tissue culture dish for 48 h. Cells were then treated with DOX for 30 min, followed by DOX wash off, and were grown further for 20 h in RPMI media without DOX before fixing with ice-cold methanol for 1 min. Cells immunostained with antibodies against Astrin and HEC1. 3D rendering was performed with Imaris 9.5.0.